Materials and Structures (2026) 59:149
https://doi.org/10.1617/s11527-026-03038-z

ORIGINAL ARTICLE

Asphalt modification using a novel bio-based amido-boron additive synthesized from waste tallow

Bahadır Yılmaz · Ahmet Münir Özdemir · Kemal Sancak

Received: 18 December 2025 / Revised: 3 February 2026 / Accepted: 25 February 2026 / Published online: 13 March 2026
© The Author(s) 2026

Abstract In this study, a novel and chemically engineered asphalt binder additive (AFBN) was developed through a multistep synthesis route incorporating waste tallow, 1,6-diaminohexane, and hexagonal boron nitride (h-BN). The originality of the additive lies in its dual-function molecular structure, comprising amide linkages and nitrogen sites capable of electrostatic interaction with boron species, designed to mimic and enhance the viscoelastic network of bituminous systems. The structural integrity and successful functionalization of the synthesized additive were confirmed through comprehensive spectroscopic techniques, including FTIR, ^{1}H-NMR (with D_2O exchange and TFA protonation), and ^{13}C-NMR, while thermogravimetric analysis (TGA) verified its thermal stability under asphalt modification conditions. The additive was incorporated into asphalt binders at varying ratios (1%, 2%, 4%, 6%) and evaluated via conventional binder tests, Brookfield rotational viscosity, and Dynamic Shear Rheometer (DSR) tests, both before and after Rolling Thin Film Oven Test (RTFOT) aging. The 2% AFBN-modified binder demonstrated superior rutting resistance and enhanced elastic behavior, as evidenced by increased $G^*/\sin\delta$ and reduced phase angle values. A multi-objective optimization study based on Response Surface Methodology (RSM) revealed that while 2% AFBN appeared optimal experimentally, a numerically optimized dose of 1.49% at 70 °C achieved a $G/\sin\delta$ of 1374.19 Pa with a desirability score of 1.0, indicating maximum rheological efficiency with reduced material input. This data-driven approach highlights the capability of statistical modeling to refine binder formulation beyond conventional trial-and-error methods.

Keywords Asphalt · Waste tallow · Modification · Rheology · Hexagonal boron nitride

B. Yılmaz · A. M. Özdemir (✉)
Civil Engineering Department, Engineering and Natural Sciences Faculty, Bursa Technical University, 16330 Bursa, Turkey
e-mail: ahmet.ozdemir@btu.edu.tr

K. Sancak
Department of Chemistry, Faculty of Science, Karadeniz Technical University, 61080 Trabzon, Turkey

1 Introduction

Waste oils are generated as a result of various industrial processes, causing ecological and biological harm. Controlling these oils is of great environmental and economic importance. To this end, numerous government strategies and academic studies have been carried out worldwide and in our country. In Turkey, 1.5 million tons of vegetable oil are used for food purposes annually, with 350,000 tons emerging as waste. Waste disposal processes are generally used for vegetable oils due to the large and varied amount of waste and the ease of the transesterification

process. Some government agencies, municipalities, and chambers of commerce and industry have undertaken various initiatives and applications for the storage or processing of waste oils. The Ministry of Environment and Urbanization also published a waste oil regulation in 2019, thereby ensuring the standardization and control of waste oil generated in facilities and businesses [1].

Animal fats are generally composed of a mixture of triglycerides, proteins, water, and various minerals. These fats are added to pet food and animal feed and are used for industrial purposes such as soap making. In addition, animal fats are preferred raw materials for biodiesel because their costs are significantly lower than those of vegetable oils. This is because the animal fat market is much more limited than the vegetable oil market. In the process of obtaining animal fats, waste oils are first extracted from animal carcasses and then converted into oil using a processing process. Most oil waste is obtained from the agricultural food industry. In addition, there is also tallow, pork fat waste, and restaurant oil waste [2–5]. For example, in the United States (US), a large portion of the animal fat waste produced is considered inedible by humans. Animal fat waste obtained from meat processing industries, tanneries, and slaughterhouses is an important source of energy and chemicals in various fields due to its renewable nature, good calorific value, chemical inertness, and zero corrosiveness. In the US, more than 1.4 billion gallons of animal fat and waste cooking oil are generated annually, and more than 74% of inedible fat and tallow is used in the production of feed, soap, and lubricants [6, 7].

Waste animal oils constitute a well-established by-product stream of the meat processing, rendering, and food industries and are routinely collected in centralized facilities. Recent assessments indicate that rendered animal fats are generated at a global scale of approximately 15 million tonnes per year, highlighting their substantial availability as a secondary raw material [8]. In the United States alone, annual production of waste animal fats and used cooking oils exceeds 1.4 billion gallons (≈5.3 million tonnes), demonstrating the robustness of existing collection and handling infrastructures [9]. At a national scale, studies focusing on Türkiye report that waste animal fats originating from cattle and sheep slaughter may reach on the order of 60–100 thousand tonnes per year, even when considering only primary rendering sources [10]. Beyond slaughterhouse-derived fats, additional contributions from food service waste, grease traps, and processing by-products further increase the overall available feedstock [11]. Importantly, the proposed bio-based amido-boron additive is applied at relatively low dosages with respect to the asphalt binder content, meaning that only a small fraction of the available waste oil streams would be sufficient to support large-scale asphalt applications. Therefore, from both a quantitative and logistical perspective, waste animal oils represent a realistic and sustainable resource for the development of bio-based asphalt additives.

In recent years, numerous studies have been conducted on the use of waste oils in asphalt mixtures [12, 13]. In particular, studies aimed at improving recycled asphalt have determined that waste oils rejuvenate the asphalt binder and reduce aging effects. Some of the waste oils used include edible oil [14, 15], motor oil [16], palm oil [17], pyrolytic oil [18], soybean oil [19], tung oil [20], and cottonseed oil [21]. There are limited studies in the literature on the use of waste animal fats [22, 23]. Waste oils have been widely preferred in the improvement of asphalt binders and mixtures; however, it has been observed that various negative effects arise when the optimal addition ratio cannot be achieved and the asphalt becomes overly young.

In recent studies, efforts have been made to obtain stronger molecular bonds by subjecting fatty acids to chemical reactions with various diamine structures. Anyaogu and his team aimed to obtain a thixotropic coating by adding various diamines to soybean oil. In this context, soybean oil was first dimerized with N_2 (nitrogen) and I_2 (iodine), and then aromatic diamines were added to this structure. After the process, it was observed that this coating structure exhibited more advanced flow properties, high storage stability, and film hardness [24]. In another study, Alam and his team reacted waste flaxseed oil with diethanolamine to obtain poly(amine-amide) resin. Emphasizing that it was obtained from a sustainable source, the study achieved high alkali resistance compared to traditional polyesteramide coatings [25]. In numerous studies like this, it has been observed that the regeneration of oils with amine and amide structures is possible, thereby forming stronger bond structures. Souza and his team conducted a study on the functionalization of castor oil with aromatic amines, emphasizing

that new molecular structures could be obtained in a simple manner. As a result of physicochemical analyses, they determined that the addition of aromatic amines to hydroxyl groups increased the thermal and oxidative stability of the compound [26].

Various studies have been conducted in the literature on the addition of boron to asphalt materials. The first studies date back to the 1940s and 1950s, but recent studies are more noteworthy. Boykin modified asphalt mixtures heated up to 210 °C with boron oxide/boron element to enable their use as neutron absorbers in radiation-absorbing barriers, neutron moderators, reactor control, and neutron reduction elements. Boric acid was used for this purpose. As a result, they noted that the boric acid added into the asphalt formed a chemical bond with the asphalt and that the asphalt mixture contained a boron oxide or boron element concentration of 1–25% [27]. Marzocchi and his team proposed reinforcing asphalt with glass fiber particles (added as fillers), but the high hydrophilic properties of glass fiber prevented it from forming chemical and physical bonds with the asphalt. To form this bond (to improve the adhesion properties of asphalt), they used a borate reaction product formed by subjecting an ortho ester, which is an organic metal compound, to a chemical reaction with a borate ester to modify the asphalt [28]. Oruç et al. stated that boron cannot be added directly to asphalt and must be bound to asphalt via a bridge. Other studies conducted by the same research team also emphasize this point. They succeeded in enhancing the rheological properties of asphalt using their original additive [29, 30].

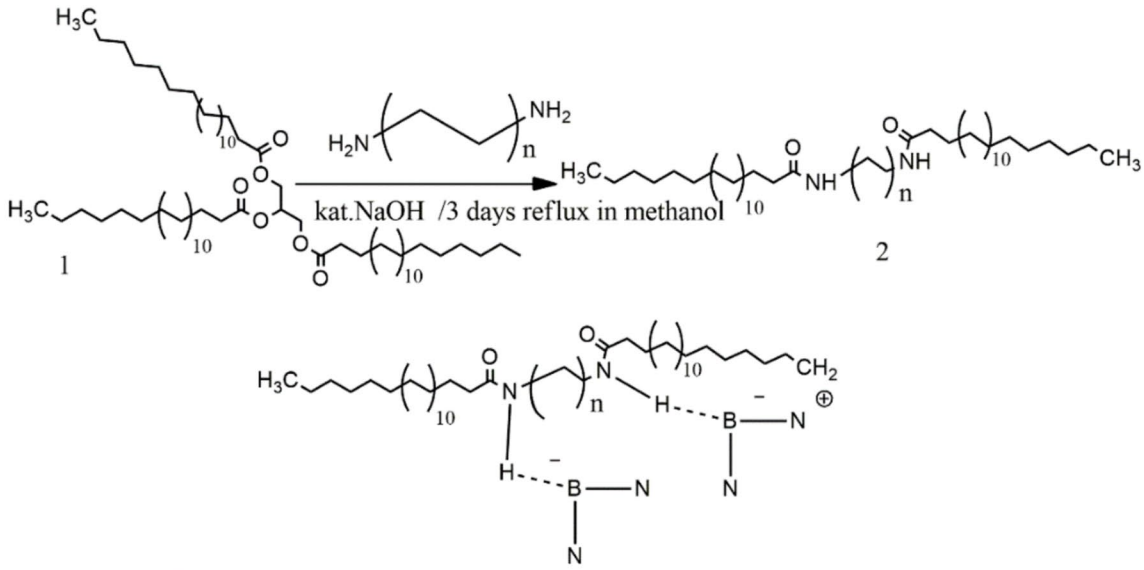
Boron nitride, a boron-based compound, plays an important role due to its thermal and chemical stability at high temperatures, its ability to exist in different forms, its cubic form being one of the hardest substances found in nature, and its optical properties. Due to these properties, it has a wide range of applications. It is preferred in various fields such as abrasive materials, thermal insulators, lubricants, and the production of defense industry equipment, and offers high potential for use in nanotechnology. Boron nitride can exist in numerous forms due to differences in the arrangement of boron and nitrogen atoms. Among these, the most stable crystalline form is the hexagonal form, known as hexagonal boron nitride (h-BN). h-BN possesses thermal conductivity and stability, ultra-high mechanical strength and hardness, impermeability, good biocompatibility, and biodegradability in nature [31–33]. There is limited literature on the use of this high-potential material in asphalt modification. Li and Wu preferred boron nitride to enhance the thermal properties of asphalt. They stated that as the BN content increases, thermal conductivity and heat diffusion coefficient also increase, which could be effective in combating snow and ice [34].

No studies have been found in the literature on the chemical treatment of animal waste oils with the addition of amines and diamines, followed by the use of the resulting additive in asphalt modification. However, it is known that animal waste oils, compared to vegetable oils, consist of fatty acids with longer carbon chains and that the saturated carbon chains in animal waste oils are more concentrated than the unsaturated carbon chains in vegetable oils, making them more compatible with the structure of asphalt. In this context, it is believed that the synthesis of a new additive containing boron nitride using waste tallow within the scope of this study will make an important contribution to the literature. Furthermore, it is believed that the additive obtained will be a low-cost and practical additive compared to the expensive and difficult-to-obtain polymer additives that are commonly used. For BN to be considered a direct asphalt additive, it must interact with asphalt. In this study, BN was used as an asphalt additive by attaching it to diamine-regenerated amide animal waste oil. It is also expected to be an additive that enhances both high and low-temperature performance, as expected from an additive. This is achieved by the hybrid presence of waste oil and BN in the modification system.

2 Materials and method

2.1 Synthesis of boron nitride reinforced additive

Figure 1 shows the general synthesis scheme of the compounds. Animal fat (waste tallow) (Compound (**1**)) (0.025 mol of oleic acid) was dissolved in absolute methanol and refluxed for 3 days under a reflux condenser and a drying agent in the presence of 1–6 diaminohexane (0.0705 mol) and a catalytic amount of NaOH (0.2 g). The precipitate was collected from the cooled solution, filtered, and dried. Compound **(2)** was obtained. The structural characterization of the compound was confirmed using FTIR, ^{1}H-NMR



Possible interaction between the additive in amidic form and boron nitride

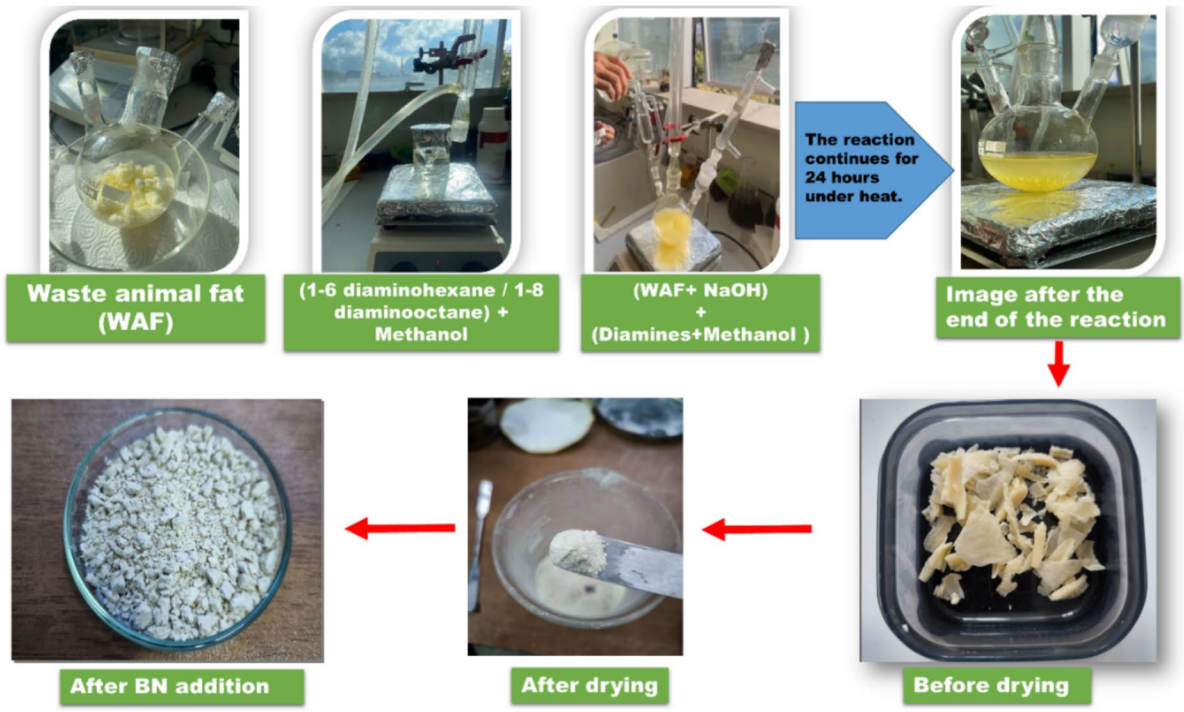


Fig. 1 General scheme of synthesised compounds and Schematisation of the additive synthesis process

(D_2O) exchange and TFA protonation), ^{13}C-NMR, and TGA.

First, 0.075 mol of animal fat was dissolved in NaOH. 24.5 g of 1–6 diaminohexane was dissolved in absolute methanol and dripped through a dropping funnel for 1 h. The system was slowly heated. The reaction was continued for 24 h, and the non-reactive portions were separated using petroleum ether. Pure water was

used to dissolve the remaining diamines. This allowed both purification and removal of excess diamines to be carried out in an inexpensive and accessible manner. The substances were then separated by filtration using filter paper. The final additive obtained had a partially oily structure. Hexagonal boron nitride (BN) was added at different percentages by weight (5%, 10%, 15%) to the 1–6 diamine + animal fat additive. The BN addition was carried out by mixing at elevated temperatures. It was observed that the final additive melted under heat and completely turned into a liquid state. However, it was noted that the material did not degrade at its melting temperature, leading to the conclusion that this was an important advantage.

The additive was dried with acetone and then ground. In the acetone drying process, the material in the first stage represents fractions composed of the relatively solid parts of animal fat. The unsaturated parts, or in other words, the parts where the double bonds first break, were used in the production of the additive. These parts are relatively solid forms such as stearic acid and oleic acid. The dried part was passed through a standard sieve. This form of the additive was named AF-6 because it contains animal fat and 1–6 diaminohexane. This structure corresponds to compound (2) in Fig. 2. In line with the main objective of the study, boron nitride was added to AF-6, and it is expected that the boron element will interact by electrostatically binding to the free orbitals of nitrogen in the diamine structure, which can be described as a "guest room." Fig. 1 shows the possible interaction scenario with BN and the synthesis process of the additive.

2.2 Preparation of modified asphalt binders

Bitumen of penetration grade B 70/100 has been liquefied at a temperature of 150 °C. A specific amount of binder has been added to the mixing container, which has been conditioned and stored at the same temperature. Based on the approximate decomposition temperatures determined by thermogravimetric analysis of the produced additives, the modification temperature was set at 160 °C. In summary, the additive and binder were mixed at 160 °C, 1000 rpm, for 1 h to obtain modified bitumen. The modification process was carried out in a mechanically stirred apparatus with four blades, where the temperature could be adjusted and maintained at a constant level.

2.3 Chemical and physical characterization methods

FTIR spectroscopy was used to characterize the chemical structure of the pure additive and the modified asphalt binders. Measurements were performed using a PerkinElmer FTIR spectrometer equipped with an ATR accessory. Spectra were recorded in the range of 4000–500 cm^{-1} at a resolution of 4 cm^{-1}, with 32 scans averaged for each measurement. Background spectra were collected prior to analysis, and all spectra were baseline-corrected and normalized before interpretation.

The chemical structure of the synthesized bio-based amido-boron additive was further analyzed by ^{1}H-NMR and ^{13}C-NMR spectroscopy using a Bruker NMR spectrometer. Samples were dissolved in a deuterated solvent and analyzed at room temperature. Chemical shifts were reported in ppm relative to the residual solvent signal.

Thermal stability of the bio-based amido-boron additive was evaluated by thermogravimetric analysis using an Exstar SII TG/DTA 6300 analyzer. Approximately 5–10 mg of sample was heated from 20 °C to 500 °C at a heating rate of 10 °C/min, and the mass loss was continuously recorded.

Morphological characterization of the additive was carried out using a ZEISS EVO LS-10 scanning electron microscope (SEM) operated at an accelerating voltage of 15 kV.

To ensure sufficient repeatability of the chemical analyses, all FTIR, NMR, and TGA measurements were conducted under strictly controlled and identical experimental conditions. FTIR spectra were recorded with multiple scans, showing consistent spectral features across measurements, while repeated NMR and TGA analyses exhibited negligible variation, confirming the reliability of the obtained results.

2.4 Laboratory ageing methods

The RTFO test is applied at 163 °C for 85 min according to the AASHTO T240 standard to simulate short-term aging in pure and modified asphalt. This process accelerates oxidation, increasing the viscosity and hardness of the binder and affecting initial performance. In modified asphalt, the test is used to evaluate the aging resistance of admixtures. In this study, the effect of the admixture on aging was investigated by performing penetration, softening point, rotational viscometer, and DSR tests after RTFO application.

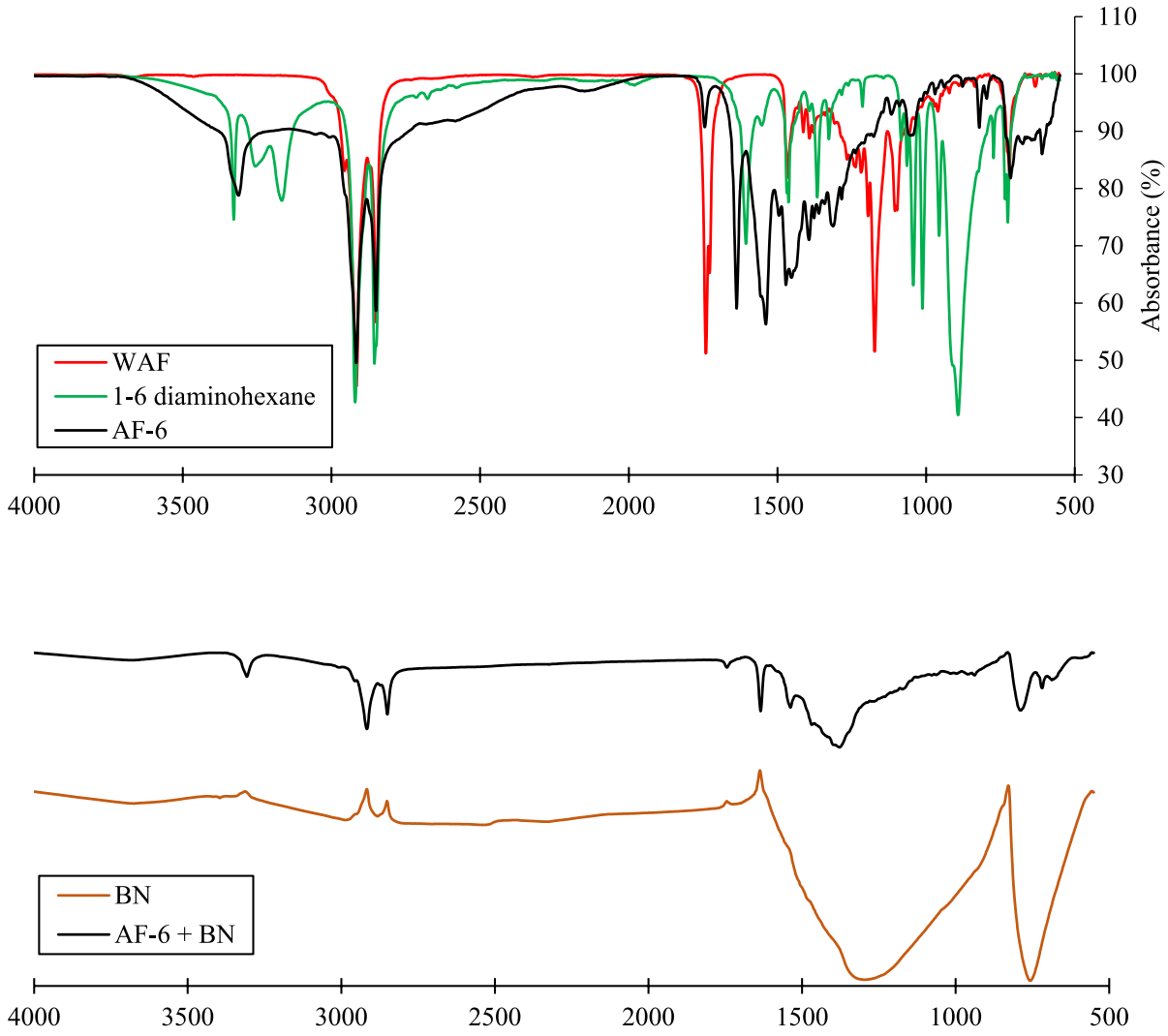


Fig. 2 FT-IR spectra of compounds used in additive synthesis

2.5 Conventional asphalt binder tests

In this study, penetration and softening point tests were used to evaluate the hardness and thermal behavior of the asphalt binder. The penetration test (TS EN 1426) determines binder hardness based on needle penetration at 25 °C under a 100 g load, while the softening point test (TS EN 1427) identifies the temperature at which asphalt softens under heating. Together, these tests provide essential information on the thermal response and performance of asphalt binders in flexible pavements.

2.6 Brookfield rotational viscometer (RV) test

Viscosity describes the resistance of asphalt binder to deformation under shear and tensile stresses and is strongly influenced by temperature due to its thermoplastic nature [35]. Since asphalt mixtures are subjected to varying temperatures during mixing and compaction, viscosity plays a critical role in ensuring proper workability and performance [36]. The Brookfield Rotational Viscosity (RV) test is widely used to assess the flow behavior of both pure and modified asphalt binders and to evaluate the effects of modifiers such as polymers or fibers. In this study,

RV measurements were conducted using a Brookfield DV-III viscometer in accordance with ASTM D4402 at a constant speed of 20 rpm and temperatures of 135 °C and 165 °C.

2.7 Dynamic shear rheometer (DSR) test

The Dynamic Shear Rheometer (DSR) test is used to evaluate the viscoelastic behavior of asphalt binders at medium and high temperatures in accordance with AASHTO T315. The main parameters obtained are the complex shear modulus (G*), which represents the overall stiffness and resistance to deformation, and the phase angle (δ), which indicates the relative elastic and viscous behavior of the binder. Lower δ values reflect more elastic behavior, while higher values indicate viscous characteristics. The rutting resistance of the binder is assessed using the G*/sinδ parameter, where higher values correspond to greater resistance to permanent deformation. In this study, DSR tests were performed on unaged and RTFOT-aged binders using 25 mm parallel plates with a 1 mm gap at an angular frequency of 10 rad/s and temperatures ranging from 52 to 76 °C. The obtained G* and δ values were used to determine the performance grade (PG) of each binder.

2.8 Response surface methodology (RSM)

Response Surface Methodology (RSM) is a statistical optimisation technique used to model and optimise the effects of multiple variables on a response [37, 38]. By employing second-order polynomial models, RSM enables efficient analysis of variable interactions while reducing the number of experimental trials [39]. In this study, RSM analysis was conducted using Design-Expert software based on the Central Composite Design (CCD) approach to investigate the effects of temperature and contribution rate and to determine the optimum contribution level. Table 1 provides information on factors and responses.,

3 Results and discussion

3.1 Chemical and physical characterisation of AF-6 additive

FT-IR, ^{1}H-NMR, ^{13}C-NMR and TG/DTA analyses of the additive obtained using waste animal fat, diamine structures and boron nitride are given in this section. Before evaluating the FTIR curves and NMR data, it is necessary to have information about the content of the waste animal fat used for the synthesis of the additive. When the literature is examined, there are many different content determinations at different rates. Table 2 presents the fatty acids found in animal fat with the highest rates [40].

FT-IR spectra of waste animal fat (waste tallow) (WAF), 1–6 diaminohexane and HY-6 are presented in Fig. 2. FT-IR spectrum data are also given in Table 3.

As shown in Table 3, the aliphatic C–H stretching vibrations belonging to the carbon skeleton in waste tallow appear at 2995, 2917 and 2850 cm^{-1}, respectively. On the other hand, the ester carbonyl (C=O) stretching band in the triglyceride ester structure is the most important esteric bands defining the oil at

Table 2 Content of animal fat [40]

Fatty acid	Chemical formula	% content
Oleic acid	$C_{18}H_{36}O_2$	44.5
Palmitic acid	$C_{16}H_{32}O_2$	29
Stearic acid	$C_{18}H_{36}O_2$	15
Linoleic acid	$C_{18}H_{32}O_2$	6.5

Table 1 Factors and responses of RSM model

Factor	Name	Units	Min	Max	Coded Low	Coded High	Mean	Std. Dev
A	Temperature	°C	52	70	−1 ↔ 52.00	+1 ↔ 70.00	61.00	6.88
B	AFBN ratio	%	0	6.92	−1 ↔ 0.00	+1 ↔ 6.00	3.00	2.55

Response	Name	Min	Max	Mean	Std. Dev
R1	G*/sinδ	953	14,017	4643.25	3956.32

Table 3 FT-IR data of the compounds

Component name	Band strengths(cm^{-1})					
	N–H	CH=CH	C-H	C=O	C–C	CH_2-CH_3 def
WAF	–	2995	2917; 2850	1741; 1728	-	1471; 1399
1–6 diaminohexane	3255;3166 (NH_2)	–	2920; 2855	1741; 1728	1606	1471; 1367
AF-6	3307	3001	2916;2849	1633	1537	1471;1399

1741 cm^{-1} and 1728 cm^{-1}. In fact, this band completely disappears in the additive obtained as a result of synthesis. As seen in the FTIR data shown for AF-6 in Fig. 3, it is observed that it shifts to 1633 cm^{-1}. As seen in the FTIR spectrum taken for 1–6 diaminohexane, the main component used in obtaining the additive, it is observed that the N–H stretching vibrations of the NH_2 group, which emerges as the most prominent band, disappears in AF-6 (Fig. 3) and is replaced by the N–H stretching vibration of the amide group.

Examination of the FTIR spectrum of AF-6 clearly confirms the proposed molecular structure of the synthesized additive. The prominent N–H stretching band at 3307 cm^{-1} represents a key indicator of successful amide formation. The vinylic CH=CH stretching band originating from oleic and linoleic acid residues was observed at 3030 cm^{-1}, while the aliphatic C-H stretching vibrations of long hydrocarbon chains (CH2 and CH3) appeared at 2916 and 2849 cm^{-1}. The characteristic amide C=O stretching band formed as a result of the synthesis was detected

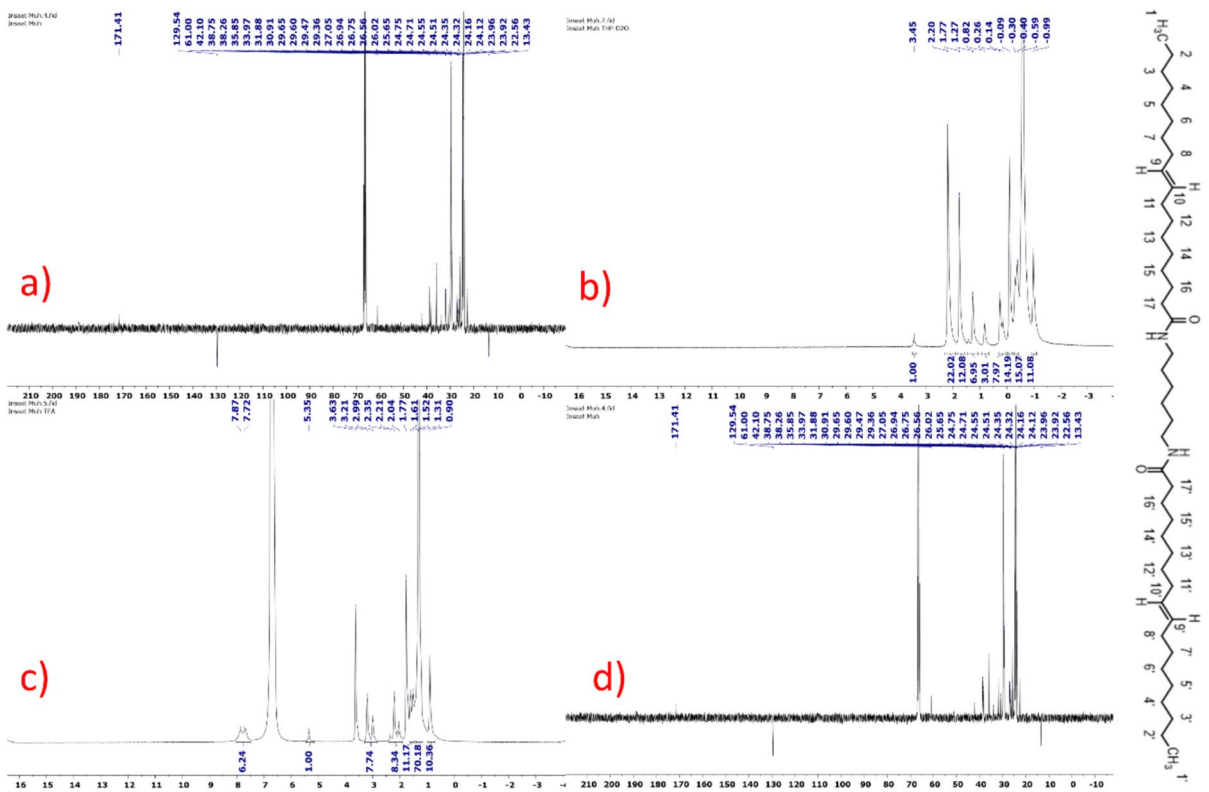


Fig. 3 1H-NMR and 13C-NMR characterization of the synthesized additive and confirmation of the proposed chemical structure **a** 1H-NMR spectrum in THF-d_8, **b** 1H-NMR spectrum in THF-d_8/D_2O, **c** ^{1}H-NMR spectrum in THF-d_8/TFA, and **d** 13C-NMR APT spectrum in THF-d_8

at 1633 cm^{-1}, accompanied by C–C stretching vibrations of the carbon backbone at 1537 cm^{-1}. Additionally, deformation bands of CH_2 and CH_3 groups were observed at 1471 and 1399 cm^{-1}. These FTIR findings strongly support the proposed additive structure and confirm the successful attachment of diamine groups to the animal fat. The residual band observed around 1740 cm^{-1} is attributed to unreacted ester groups remaining from the starting animal fat.

According to Fig. 3, there are two main bands clearly in the FTIR spectrum taken for hexagonal boron nitride. One of these is the in-plane B-N stretching vibration at 1300 cm^{-1}, and the other is the out-of-plane bending vibration corresponding to the B-N-B bond that occurs at 756 cm^{-1}. The BN ratio in the additive is 10%. The preliminary study carried out to determine this ratio is given in the following sections of the article. In Fig. 4, it is observed that the in-plane B-N stretching vibration of pure BN at1300 cm^{-1} shifts significantly and appears at 1376 cm^{-1}, while the out-of-plane bending vibration corresponding to the B–N–B bond that occurs at 756 cm^{-1} also shifts to 788 cm^{-1}. This result shows us that the NH–CO groups in the additive interact with boron nitride in the form of B–N–N. Parallel to these data, information is reported in the literature that there is a B–N–N interaction between boron nitride and nitrogen-containing compounds [41]. One of the main motivations of the

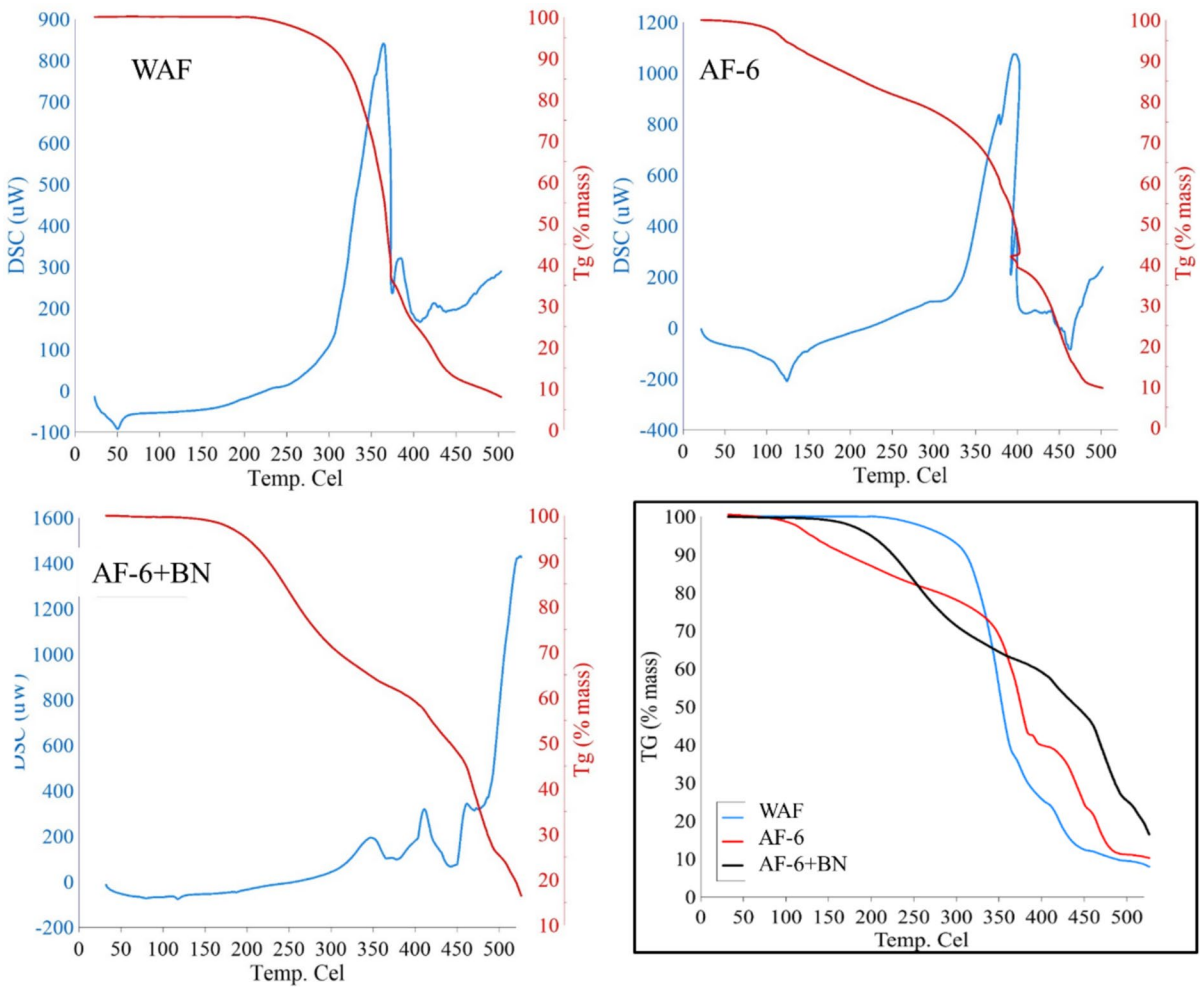


Fig. 4 Thermogravimetric analysis results of additives

Table 4 ^{1}H-NMR data of the additive

CH_3 (1–1')	0.94, s, 6H
CH_2 (2–2'), CH_2 (3–3'), CH_2 (4–4'), CH_2 (5–5'), CH_2 (7–7'), CH_2 (12–12'), CH_2 (14–14'), CH_2 (15–15')	1.34–1.62, m, 32H
CH_2 (6–6'), CH_2 (13–13'), –N–CH_2–CH_2	1.78–2.08, m, 12H
-N–CH_2–CH_2–CH_2, CH_2 (16–16')	2.31–2.65, m, 8H
CH_2 (8–8') CH_2 (11–11'), CH_2 (17–17')	3.17, s, 12H
–N–CH_2	3.34, s, 4H
CH = CH (9–9'), CH = CH (10–10')	5.37, s, 2H
–N–H	6.78, s, 2H

study is to synthesize an additive that is one-to-one similar to the asphalt binder. As mentioned before, the reason why animal fat was preferred in the study is that it has longer carbon chains compared to vegetable oil and that the saturated parts are found in higher ratios than the unsaturated parts. It is thought that the relationship between the additive and the asphalt binder is based on electrostatic attraction forces. In addition, as mentioned above, it is thought that boron nitride is connected to the additive with a possible B–N–N interaction. Indeed, important spectral data confirming this idea were obtained in the boron-doped material. It is possible that the boron element is included in the system via the free orbitals in the nitrogen atom. Figure 3 presents the NMR characterization of the synthesized additive and its proposed chemical structure. Figure 3(a) shows the ^{1}H-NMR spectrum of the additive recorded in THF-d_8, with characteristic solvent peaks at 1.77 and 3.63 ppm. Figure 3(b) displays the ^{1}H-NMR spectrum obtained in a THF-d_8/D_2O mixture, demonstrating the exchangeable protons in the structure. Figure 3(c) illustrates the ^{1}H-NMR spectrum recorded in a THF-d_8/TFA mixture, highlighting protonation effects and further confirming the presence of amide functionalities. Figure (d) presents the ^{13}C-NMR APT spectrum of the additive in THF-d_8, providing detailed information on the carbon framework of the target compound. Together, these spectra confirm the proposed molecular structure of the synthesized additive.

Each atom was named and used in the evaluation of the NMR analysis. In addition, the ^{1}H-NMR data of the additive are given in Table 4.When Fig. 3 was examined, it was evaluated that the most important data regarding the contribution was the emergence of NH proton signals at 6.78 ppm in a very low area, indicating that amidation was achieved. In addition, the proton signal at 5.37 ppm reveals the CH = CH unsaturation of oleic acid and linoleic fragments in the oil body. The ^{1}H-NMR spectrum obtained as a result of the isotope exchange of the additive with D_2O (deuterated water) revealed remarkable behaviors. Indeed, in the ^{1}H-NMR spectrum given in Fig. 4, it is observed that the N–H proton signal that emerged at approximately 6.67 and 6.78 ppm has completely disappeared from the spectrum. This behavior is expected in protons attached to strongly electronegative atoms. This behavior definitely confirms the presence of an amidic NH. Due to the shift of the standard 0 (zero) point in the spectrum to a slightly higher area, the proton signals belonging to the CH = CH group are recorded at 3.45 ppm, while the real value is seen to be 5.43 ppm. This spectrum was made to determine the NH protons.

Since the most important data indicating that the targeted contribution is formed is the NH protons, in order to make additional confirmation of the NH protons, the formation of the amidinium cation by additional protonation of the NH protons in TFA (trifluoroacetic acid) and the shifting of the proton signals belonging to this cation to the downfield were aimed. As a matter of fact, as seen in the spectrum given in Fig. 3, the peaks observed at 6.67 and 6.78 ppm in the spectrum above shifted to the downfield as 7.72 and 7.87 ppm, which is presented as data that absolutely confirms the structure.

The most important spectral data indicating that the targeted contribution has been achieved is the observation of the carbon peak belonging to the amidic C = O group at 171.41 ppm in the lowest area. In addition, the carbon peaks belonging to the CH = CH group in the carbon chain of some triglyceride esters (oleic acid and linoleic acid) in the oil structure appear at 129.54 ppm in the lower area

Table 5 ^{13}C-NMR spectral data

$C(CH_3)$ (1–1') (13.43); $C(CH_2)$ (2–2')(22.56); $C(CH_2)$ (3–3') (23.92); $C(CH_2)$ (4–4')(23.96); $C(CH_2)$ (5–5') (24.12); $C(CH_2)$ (6–6') (24.16); $C(CH_2)$ (7–7') (24.32); $C(CH_2)$ (12–12') (24.35); CH_2 (13–13') (29.65); $C(CH_2)$ (14–14') (24.51); $C(CH_2)$ (15–15') (24.55); $C(CH_2)$ (16–16') (25.65)	
–N–CH_2–CH_2–CH_2, CH_2 –CH_2–CH_2–N	$C(NCH_2$(42.10)
–N–CH_2-CH_2–CH_2, CH_2 –CH_2–CH_2 –N	$C(C–CH_2$(30.91)
–N–CH_2–CH_2–CH_2,CH_2 –CH_2–CH_2 –N	$C(C–CH_2$(26.56)
$C(CH_2$-CH = CH) (8–8')(31.88), (CH_2 (11–11') (33.97), $C(CH_2)$ (17–17') (38.75)	
C(CH = CH) (9–9'; 10–10') (129.54)	
C(C = O) (171.41)	

as expected. The CH_2 and CH_3 group carbon peaks belonging to the oil chain and amide chain presented in the table are presented in detail in Table 5. The relevant data confirm the targeted compound.

Thermogravimetric analysis results of waste tallow, AF-6 and AF-6 + BN additives are given in Fig. 4.

Figure 4 presents the TGA curves of waste tallow, the synthesized additive (AF-6), and the boron nitride-modified additive (AF-6 + BN). Waste tallow exhibited nearly 90% mass loss, while AF-6 showed earlier thermal degradation, which could be unfavorable for asphalt modification temperatures. However, the addition of hexagonal boron nitride significantly improved thermal stability, shifting the onset of decomposition to higher temperatures and leaving nearly 20% residue. Overall, the TGA results confirm that AF-6 + BN is thermally stable at asphalt modification temperatures and that boron nitride effectively enhances the thermal resistance of the additive. The thermal resistance of hexagonal boron nitride is mentioned in detail in the literature [42, 43].

3.2 Determination of the ideal BN ratio to be used for additive synthesis

In the additive to be obtained, first 10% boron nitride was used, after the structural characterization was completed, various performance experiments were carried out on the asphalt binder to determine the ideal ratio. In this context, each additive was added to the asphalt binder at a weight rate of 2%. 3 different additives containing BN at 5%, 10% and 15% were synthesized. In addition to these binders, the same amount of this additive was added to see the effect of the additive that does not contain boron nitride. Penetration, softening point and dynamic shear rheometry (DSR) experiments were carried out on the modified asphalt binders, the results are given in Fig. 5.

When Fig. 5 is examined, it is seen that the use of additives reduces the penetration value of pure asphalt. It is thought that the diamine structures in HY-6 cause hardening in asphalt. When the BN ratios are examined, it is seen that the penetration values decrease in all three BN ratios compared to pure asphalt, and the additive increases the consistency of the asphalt. The lowest penetration value was seen in the 10% BN ratio, and this trend was reversed after the addition of 15% BN. According to the penetration test results, the ideal BN ratio was determined as 10%. According to Fig. 5, the highest softening point value was obtained in the additive with 10% BN addition. It is pleasing that higher values were observed in all other additives compared to the pure binder. According to the softening point test results, the ideal BN ratio was determined as 10%. Except for the HY-6 binder, all other binders presented higher G* values compared to pure asphalt. With the increase in the BN ratio, G* values increased, but this increase was reversed at the 15% BN ratio. Compared to pure asphalt at 52 °C, 5% BN binder provided 10.09%, 10% BN binder 48.09%, and 15% BN binder 18.44% higher G* values. All these results showed that the ideal BN ratio was 10%. As a result of laboratory tests, it was decided to add the additive to the asphalt binder at 1%, 2%, 4%, and 6%.

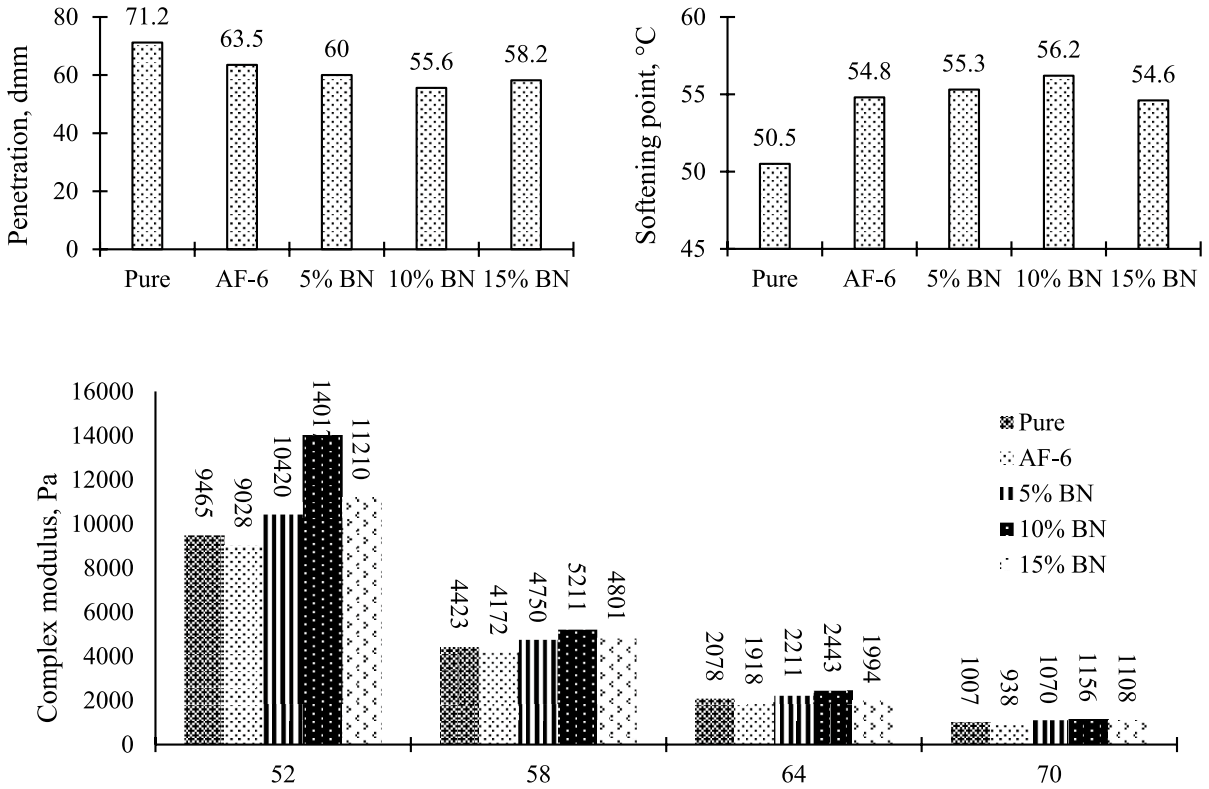


Fig. 5 Results of the preliminary study carried out to determine the ideal BN ratio

3.3 Chemical characterization of modified asphalt binders

It is important to perform the chemical characterisation of asphalt binders in order to reveal the role of the additive. For this purpose, spectrometer curves obtained from pure and 6% modified asphalt binders are given in Fig. 6.

In order to address the interaction between the bio-based amido-boron additive and the asphalt binder matrix, ATR-FTIR analyses were additionally performed on the modified binders. As shown in Figure X and Table X, the characteristic aliphatic hydrocarbon bands at 2920 and 2852 cm^{-1}, as well as the CH_2/CH_3 deformation bands in the range of 1455–1376 cm^{-1}, remained unchanged after modification, indicating that the fundamental hydrocarbon structure of the binder was preserved. However, the appearance of a distinct N–H stretching band at approximately 3307 cm^{-1} in the binder containing 6% additive confirms the successful incorporation of amide functional groups into the binder matrix. Moreover, the shift of the C = O stretching band from 1598 cm^{-1} in the neat binder to 1636 cm^{-1} in the modified binder suggests the presence of physical interactions, such as hydrogen bonding or dipole–dipole interactions, between the additive and asphalt components. FTIR measurements were conducted following rigorous sample preparation and measurement practices to ensure spectral reliability and reproducibility, in line with recent RILEM recommendations for ATR-FTIR analysis of bituminous binders (@@@). These findings provide a clear chemical link between the additive structure and the observed mechanical and rheological performance enhancements.

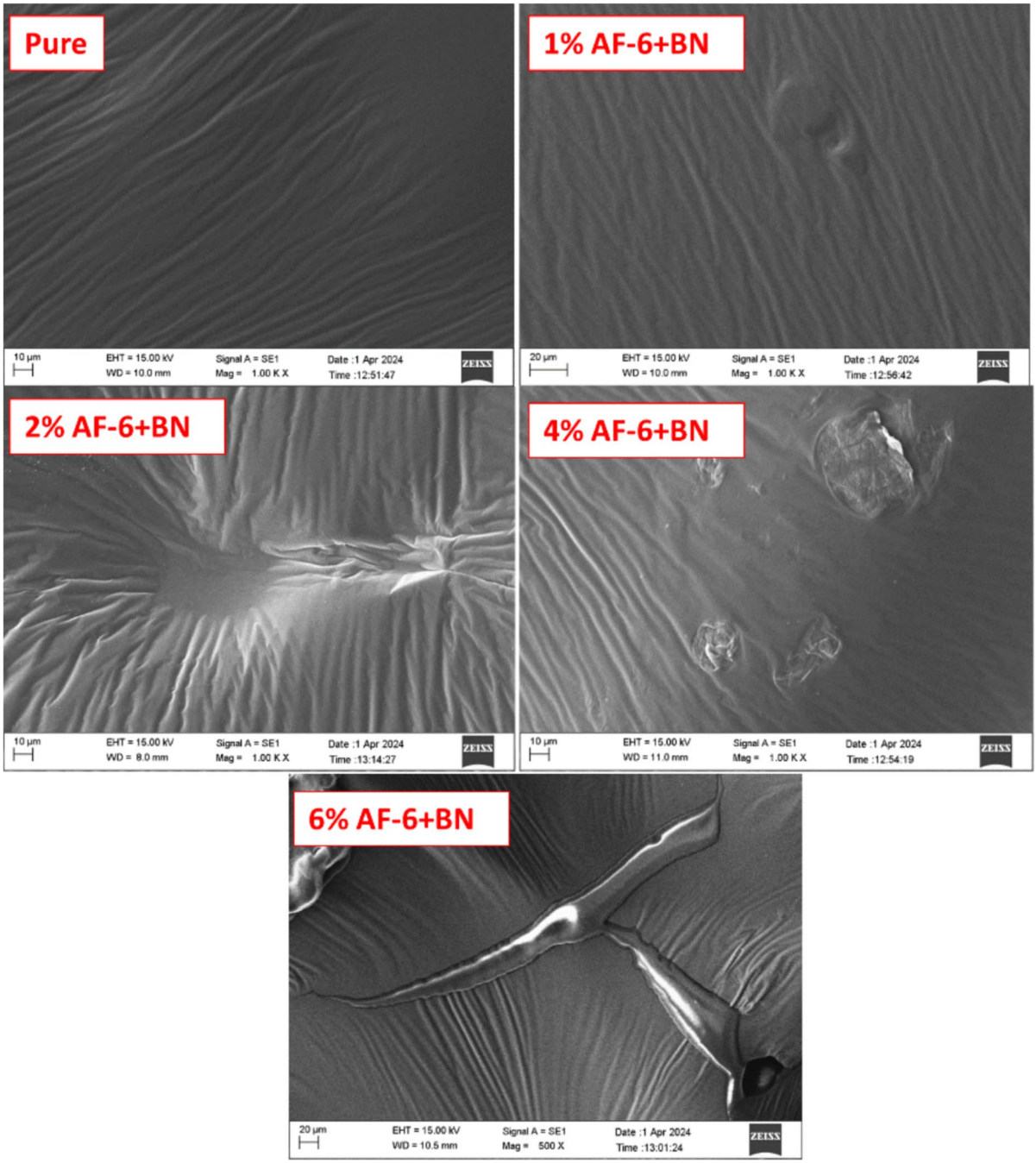


Fig. 6 SEM images of pure and modified binders

3.4 Scanning electron microscopy (SEM) results of modified asphalt binders

Scanning electron microscope (SEM) analysis was performed to determine whether the additive was distributed homogeneously in the asphalt binder and whether any structural or surface problems occurred. The results are given in Fig. 6.

The SEM images presented in Fig. 6 comparatively reveal the microstructural morphologies of pure

binder and binders containing different proportions of additives. While the pure asphalt surface has a homogeneous, fluid and continuous structure, this structure was largely preserved with 1% AFBN addition, and only micrometric level disorder was observed on the surface. At 2% additive rate, it was observed that the additive was effectively incorporated into the binder matrix and radial deformation patterns were formed from the center to the periphery. This shows that the additive increases microstructural interaction and suggests that it may contribute positively to mechanical performance. However, at 4% additive rate, significant agglomerations and lumps were formed, and surface homogeneity began to deteriorate. At 6% AFBN rate, widespread crack formations and irregular deformations were observed in the microstructure, indicating that the structural integrity of the binder was damaged and the additive was not effectively distributed in the binder matrix. These microscopic findings show that the optimum additive ratio is around 2%, and higher ratios cause negative effects by causing deterioration in the internal structure of the binder. In general, it was determined that the use of 1% and 2% additives and the modification conditions (1000 rpm, 160 °C and 1 h) were appropriate and the additive was homogeneously distributed in the asphalt binder.

3.5 Conventional asphalt binder tests results

In this section, the results of conventional asphalt binder tests are given to reveal the effect of the

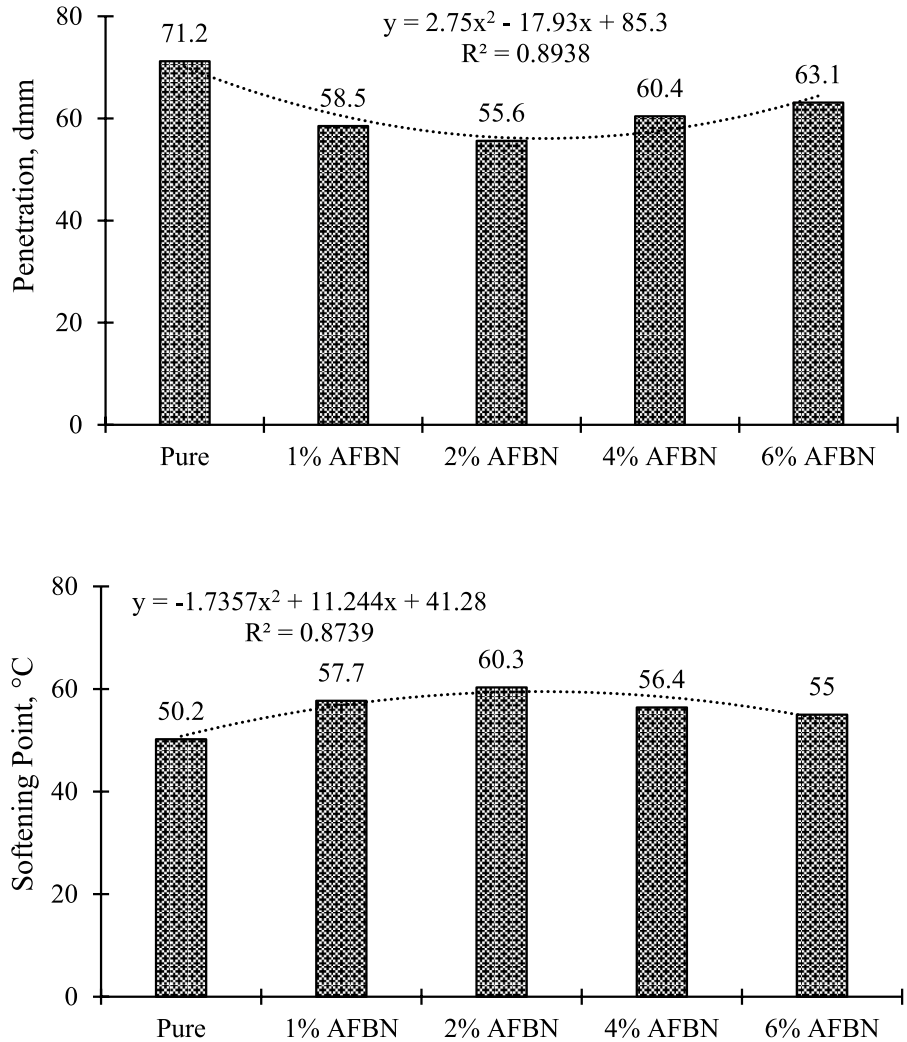


Fig. 7 Penetration and Softening point test results of pure and AFBN modified binders

synthesized additive on asphalt binder performance. In the rest of the study, the AF-6 + BN additive is called AFBN. The penetration and Softening point test results are presented in Fig. 7.

According to the results obtained, a significant decrease was initially observed in the penetration values with the addition of AFBN to the binder, and this decrease reached a minimum level (55.6 dmm) at 2% additive rate. This indicates an increase in the hardness of the binder and therefore the structural modification effect of AFBN. However, as the additive rate increased above 2%, an increase in the penetration values was observed again, reaching 63.1 dmm at 6% additive rate. According to Fig. 7, it was seen that the penetration values decreased for 1% and 2% additive rates, and this increase was reversed for 4% and 6%. The equation obtained with the second-order regression model ($R^2 = 0.8938$) strongly represents this non-linear relationship. While the penetration value decreased by 17.84% in the use of 1% additive compared to the pure binder, this situation was 21.91% at 2%. Lower penetration values were obtained compared to the pure binder at all additive rates. In general, the lowest penetration values were obtained with the addition of 2% additive, and the consistency of the asphalt binder increased significantly.

The softening point value is defined as the temperature at which asphalt becomes viscous and loses its properties. When Fig. 7, where the softening point values of the binders are given, is examined, it is seen that the highest softening point value is obtained in the binder containing 2% additive. The softening point value increased in all samples compared to pure asphalt, and this increase was determined as 14.94%, 20.12%, 12.35% and 9.56%, respectively, according to the additive content. The obtained second-order regression model ($R^2 = 0.8739$) strongly represents the non-linear relationship between the softening point and the additive ratio. These findings emphasize the importance of determining the AFBN additive ratio at the optimum level in order to improve the high temperature performance of the binder. When the penetration and softening point test results were evaluated in general, it was seen that there was a decrease in penetration values and an increase in softening point values with the addition of the additive. This situation shows that the additive will increase the consistency and hardness of the asphalt and provide resistance against permanent deformations.

3.6 Brookfield rotational viscometer (RV) test results

The viscosity values of pure and modified asphalt binders at different temperatures (135 °C, 165 °C) were found and are presented in Fig. 8.

When Fig. 8 is examined, asphalt binders containing additives at both temperatures presented higher viscosity values compared to the pure binder.

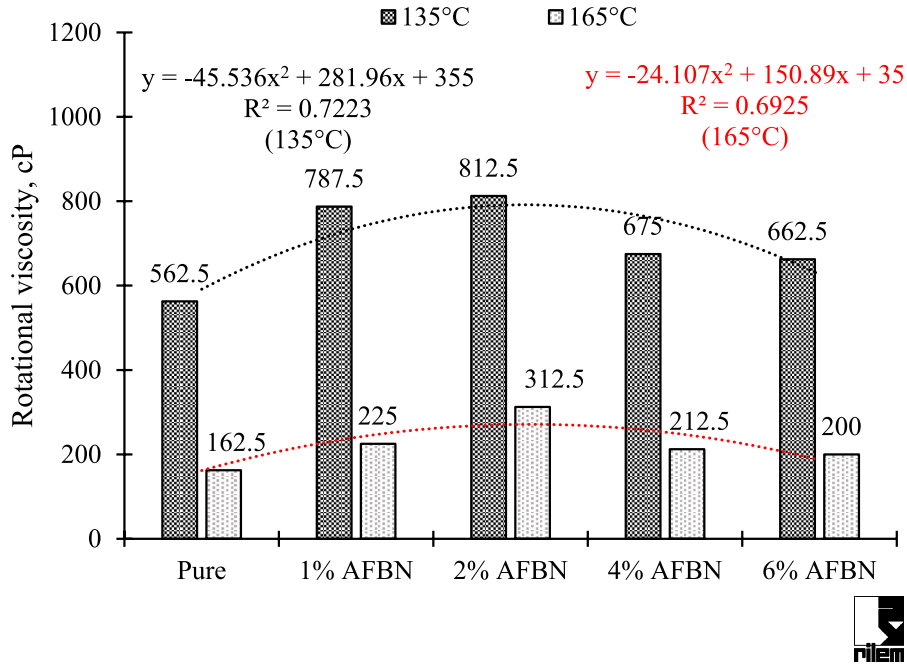


Fig. 8 RV test results of pure and AFBN modified binders

The highest viscosity value was seen in asphalt containing 2% additive. The viscosity values of pure asphalt at 135 °C were determined as 40%, 44.4%, 20% and 17.78% at 1%, 2%, 4% and 6% additive content, respectively. At 165 °C, they were 38.46%, 92.31%, 30.77% and 23.08%. No binder exceeded the specification value of 3000 cP. Significant viscosity increases occurred at 1% and 2% additive contents. This shows that the high temperature resistance of asphalt increases with the addition of additives and that it gains resistance against permanent deformation. Studies in the literature show that adding various oils to asphalt will soften asphalt. Considering the content of the additive in this thesis, it can be said that the oily part turns into a reaction product and shows a completely different feature.

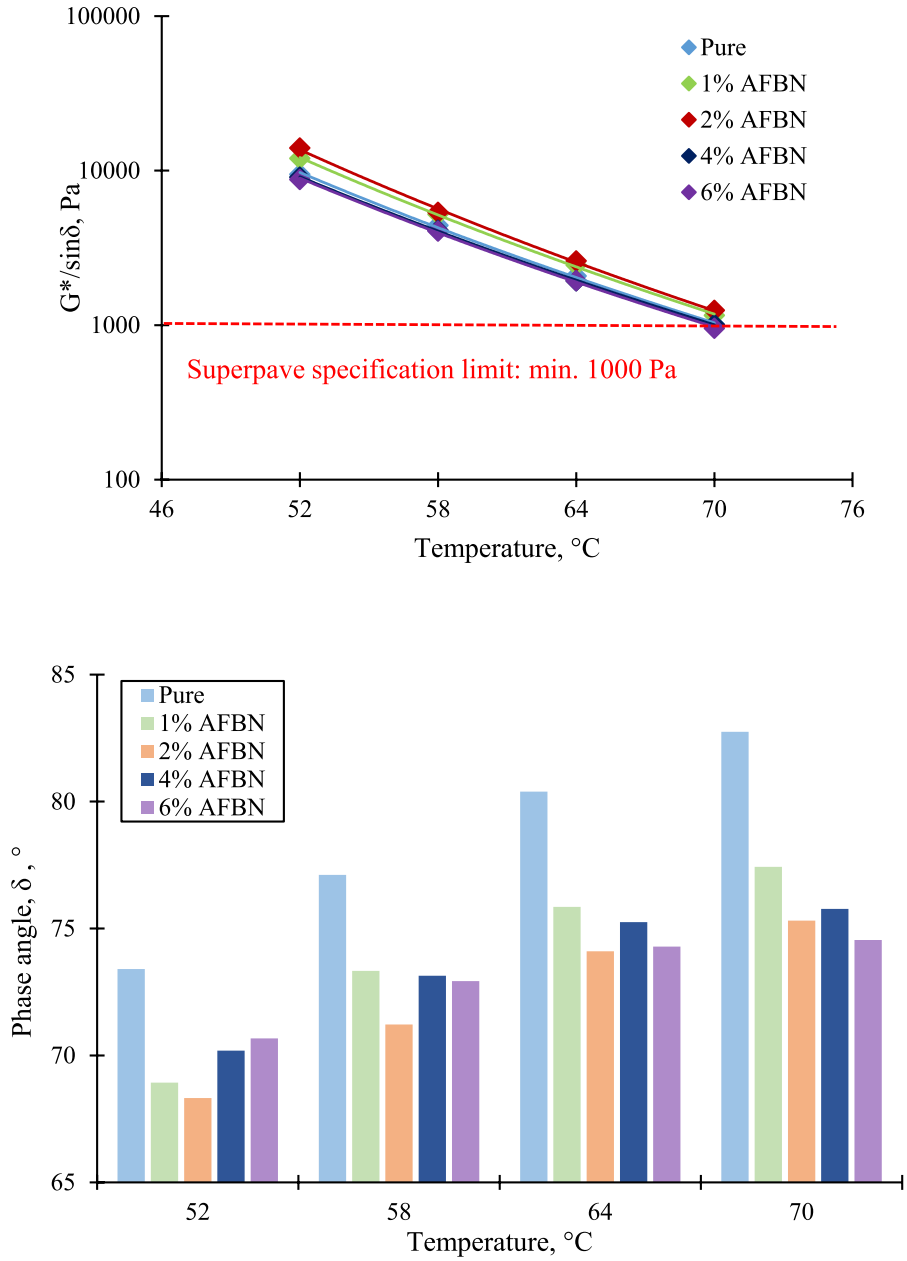


Fig. 9 G*/sinδ and phase angle results of pure and AFBN modified binders

3.7 Dynamic shear rheometer (DSR) test results

The DSR test was carried out at 52 °C, 58 °C, 64 °C and 70 °C at a frequency of 1.59 Hz (10 rad/s) using 25 mm plates and a 1 mm gap between the plates. As a result of the test, the G*/sinδ value, which is a measure of the resistance of asphalt binders to rutting, was obtained. The elastic modulus (G'), viscous modulus (G"), complex modulus (G*) and phase angle (δ) values required for the calculation of this parameter are also provided by the DSR software. The G*/sinδ and phase angle results are given in Fig. 9.

When Fig. 9 is examined, it is seen that the complex modulus values in all binder samples decrease with increasing temperature. This decrease is limited with the use of 1% and 2% additives, and higher complex shear modulus values are obtained at each temperature compared to the pure binder. This situation is reversed at 4% and 6% additive contents, and lower G* values are observed than the pure binder. The highest G* values are obtained in the binder containing 2% additive. When the phase angle values are examined, it is seen that the phase angle values also increase with increasing temperature, and the highest phase angle values are obtained in the pure binder at each temperature. The increase in the complex modulus and the decrease in the phase angle values at the same time are interpreted as the development of the elastic properties of asphalt binders. The phase angle represents the time between the application of load and the formation of deformation, and the decrease in this value indicates that the material becomes elastic. While the G* values increase significantly at 1% and 2% additive rates, the phase angle values also decrease. At other additive rates, the phase angle values show a relatively elastic behavior, but the low values seen in the complex modulus values limit this performance.

According to the Superpave specification, the G*/sinδ value must be above 1000 Pa and the last temperature that provides this value indicates the PG of the binder. When Fig. 9 is examined, it is seen that the binder containing 6% additive does not meet the 1000 Pa condition at 70 °C, while all other binders meet this condition. If the evaluation is made specifically for 1% and 2% additive rates, it is determined that no negativity is experienced in terms of PG. In general, it was concluded that the elastic properties of the asphalt improved significantly with the use of 1% and 2% additives and the rutting resistance increased. The fact that the phase angle values were significantly lower than the pure binder at all additive rates was evaluated as an indicator that the material became elastic. No negativity was observed in the PGs of the binders. Since the additive contains oil, this situation was considered positive. It is known in the studies in the literature that the addition of oil to asphalt causes a softening effect and causes quite serious problems in terms of high temperature resistance. Since the main motivation of this study is to obtain an idealized additive that will increase both high and low temperature performance, the DSR results are pleasing. Also, the phase angle values confirm this.

3.8 Rolling film thin oven test (RTFOT) results

RTFOT test was applied to evaluate the effect of the additive on the short-term aging of the asphalt binder, and penetration, softening point and DSR tests were applied to the asphalt binders subjected to RTFOT. The results of the conventional binder tests after RTFOT are given in Table 6.

When Table 6 is examined, it is seen that the penetration values for 1% and 2% rates decrease depending on the increasing additive rate, and this decrease is reversed for 4% and 6% rates and similar to the pre-RTFOT test results are obtained. While the permanent

Table 6 Test results before and after RTFOT

	Pure		%1		%2		%4		%6	
RTFOT	Before	After	Before	After	Before	After	Before	After	Before	After
Penetration	71.2	41.5	58.5	36.4	55.6	34.1	60.4	38.8	63.1	40.3
Retained Penetration (%)	58.29		62.22		61.33		64.24		63.87	
Softening P	50.2	56.4	57.7	63.5	60.3	67.5	56.4	61.9	55	60.7
ΔS (°C)	6.2		5.8		7.2		5.5		5.7	

penetration value of the pure binder is 58.29%, it is obtained as 62.22% at 1% additive rate, 61.33% at 2% additive rate, 64.24% at 4% additive rate and 63.87% at 6% additive rate. The lowest penetration value is obtained in the binder containing 2% additive, while the highest value is seen in the pure binder. Again, according to Table 6, the softening point values have increased visibly at 1% and 2% additive rates, and higher softening point values are obtained in other binder samples compared to pure asphalt. Compared to the pure binder, there is an increase of 12.59% at 1% additive rate, 19.68% at 2% additive rate, 9.75% at 4% additive rate and 7.62% at 6% additive rate. When the ΔS values in Table 6 are examined, it is seen that the softening point temperature differences decrease at all rates except for the 2% additive rate compared to pure asphalt. This situation shows that the molecules in the functional groups of asphalt undergo structural

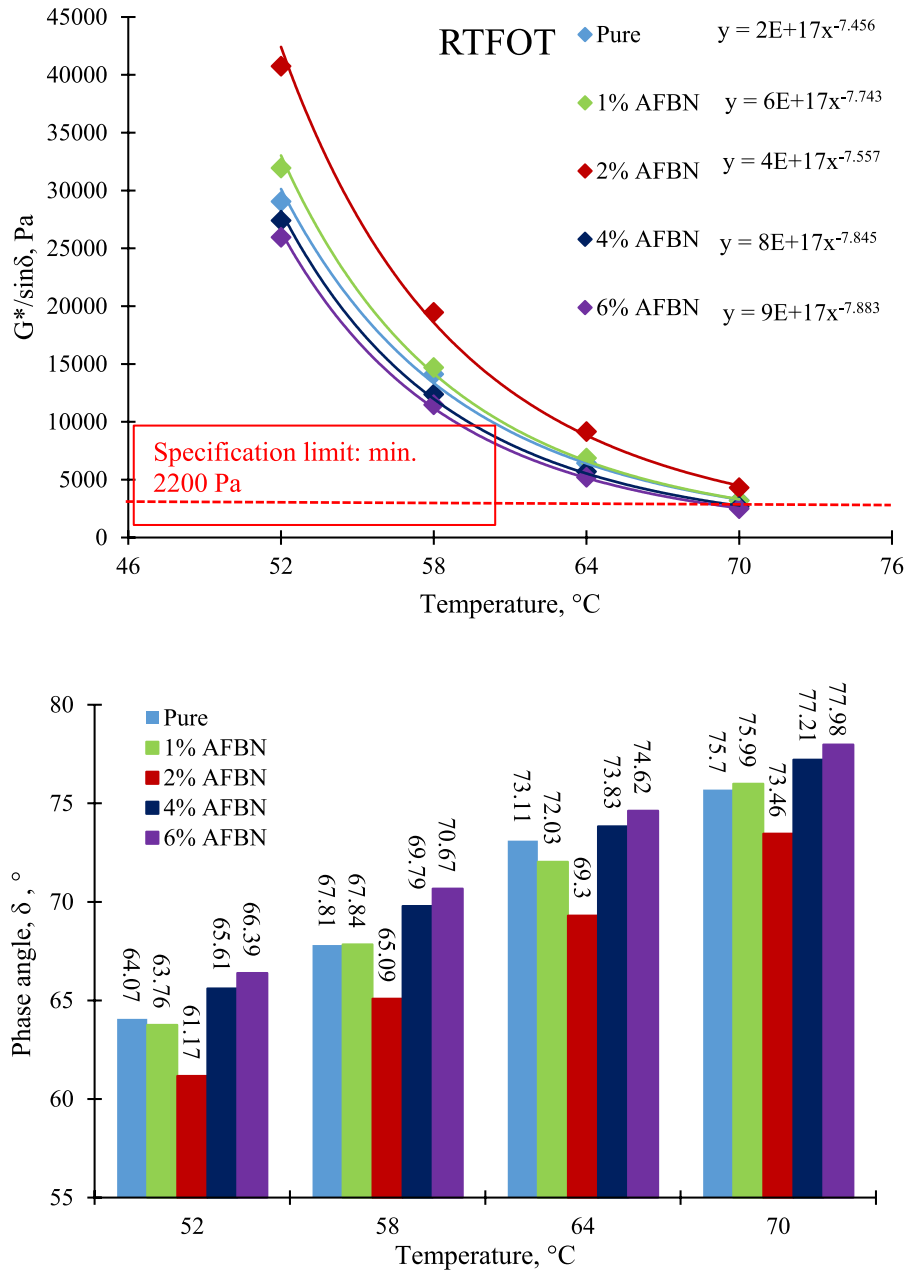


Fig. 10 G*/sinδ and phase angle values after RTFOT

changes during oxidative aging. The softening point and penetration experiments after RTFOT show that the use of additives increases the resistance to aging. It is thought that this situation is due to the oily part in the additive. The G*/sinδ and phase angle values after RTFOT are given in Fig. 10.

As shown in Fig. 10, G* and G*/sinδ values increased markedly at 1% and 2% additive contents compared to the pure binder, but decreased at 4% and 6%. All binders satisfied the specification limit of 2200 Pa at 70 °C, with the 2% AFBN-modified binder exhibiting the highest G*/sinδ value. At this temperature, changes of −0.97%, +35%, −17%, and −22% were observed for 1%, 2%, 4%, and 6% additive ratios, respectively, relative to the pure binder. These results confirm that a 2% additive content provides the optimum improvement in high-temperature elastic properties and rutting resistance after aging, which is also supported by the lowest phase angle values observed for this binder. Higher additive contents (4% and 6%) produced results similar to the pure binder, likely due to the higher oily fraction, which softens the binder and limits hardening during aging. While the specification limit was not exceeded, the presence of the oily structure suggests potential improvements in low-temperature performance and aging resistance.

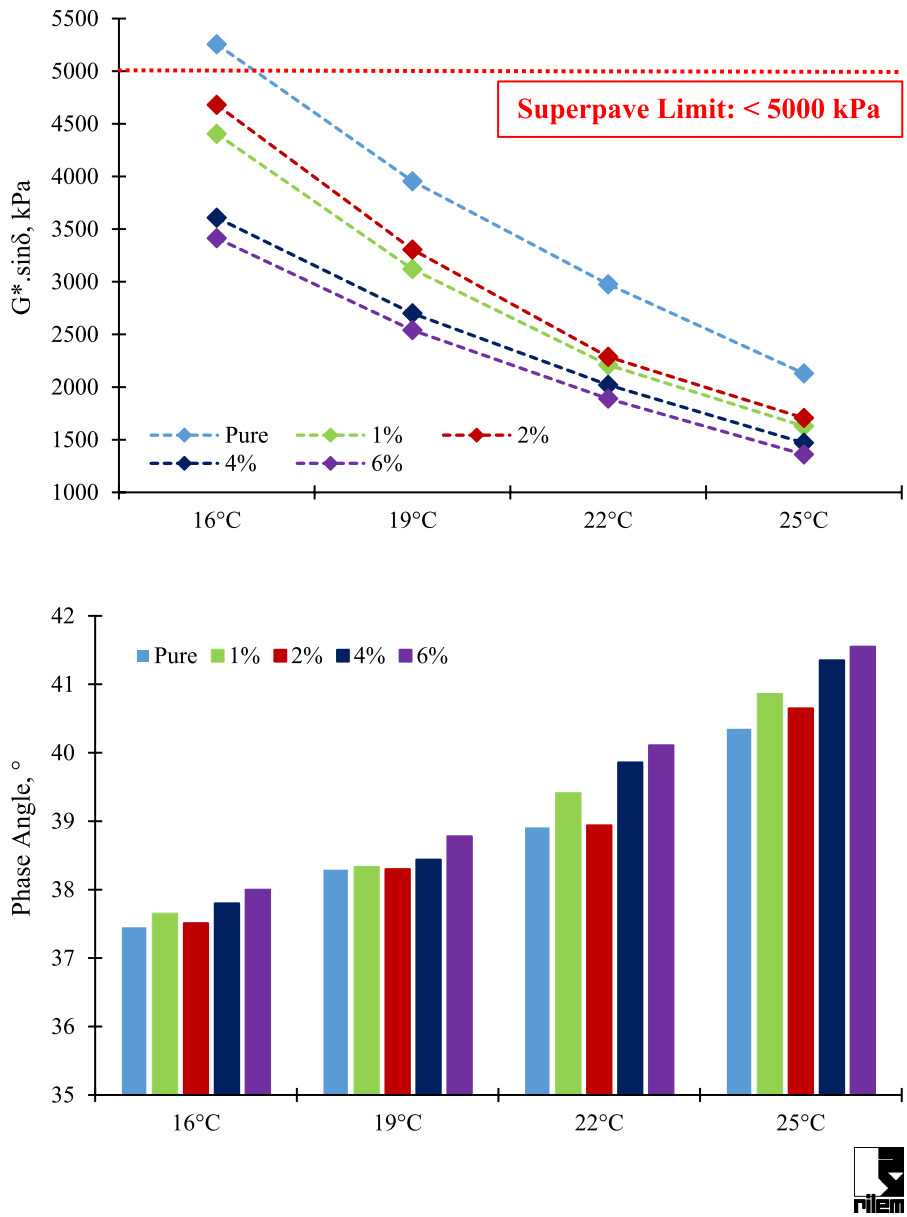


Fig. 11 G*.sinδ and phase angle values of pure and modified binders after the PAV test

3.9 Pressure ageing vessel (PAV) results

The PAV experiment simulates the long-term aging process, and DSR test was performed on PAV samples. DSR experiment data of pure and modified binders after the PAV experiment are given in Figs. 11.

The parameter G*.sinδ, examined in the DSR test results, provides definitive information about the long-term performance, or fatigue behavior, of asphalt pavements in a laboratory setting. This value is related to the fatigue performance of the pavement because it is applied to long-term aged samples. To explain its relationship to fatigue: To carry the loads applied to the asphalt pavement without cracking, a binder with softer elastic properties is needed. For this, the G* and phase angle from the DSR results need to be reduced. Therefore, the product of these two values indicates fatigue. According to the Superpave asphalt binder specification, the G*.sinδ value must be less than 5000 kPa. It has been observed that binders aged with admixtures exhibit softer elastic properties at relatively low temperatures compared to the pure asphalt binder. This is also evident from the phase angle (δ) values given in Fig. 11. Figure 11 shows that as the temperature increases, the phase angle values of all binders increase, and that lower or closer phase angle values are obtained with 2% additive content compared to pure asphalt binder. Phase angle values are considerably higher with other additive ratios compared to pure asphalt binder. While the G* value is lower with other additive ratios compared to pure asphalt binder, the same cannot be said for the phase angle values. Figure 11 shows the G*.sinδ values, which are the Superpave fatigue criteria. At 16 °C, the pure binder could not meet the specification limit of 5000 kPa. However, all other additive ratios remained below this value, meeting the specification limits. At every temperature, the pure binder provided the highest G*.sinδ value, while the lowest results were obtained with the asphalt binder containing 6% additive. The fact that all modified binders exhibited lower G*.sinδ values indicates that the addition of the additive softens the resistance (elasticity) to fatigue cracks that occur in the pure asphalt binder and develop during the service life of the pavement, thereby increasing aging resistance. However, this softening elasticity effect should be limited. At a 2% additive rate, this softening elasticity effect was limited, G*.sinδ valueswere obtained that were higher than all other binders, and most importantly, phase angle values were obtained that were quite close to or relatively lower than those of the pure binder. This shows that at a 2% additive rate, the material can withstand the applied loads without causing brittle fractures, its fatigue performance is improved, and its resistance to aging is enhanced.

3.9.1 Response surface methodology (RSM) results

RSM analysis was performed using G*/sinδ values of pure and modified binders to determine the optimum AFBN ratio. As a result of detailed analysis, the highest prediction accuracy values were obtained in the qubic model with the lowest error. ANOVA results are given in Table 7.

The ANOVA results of the model are presented in Table 7 and indicate that the model is statistically significant and reliably represents the experimental data ($F = 176.58$, $p < 0.0001$). Both main effects, temperature (A) and AFBN ratio (B), were found to be significant with F values of 497.09 ($p < 0.0001$) and 16.69 ($p = 0.0015$), respectively, while their interaction (AB) was not significant ($p = 0.5384$). Among the higher-order terms, A^2, B^2, and B^3 were significant, revealing a strong nonlinear relationship with the response, whereas AB^2 showed borderline significance. The high R^2 (0.9904), adjusted R^2 (0.9848), and predicted R^2 (0.965) values confirm the excellent fit and predictive capability of the model. Additionally, the Adeq Precision value of 37.95 demonstrates an adequate signal-to-noise ratio. Overall, the results confirm that temperature and AFBN ratio significantly influence the rheological properties of the asphalt binder, and the developed model is suitable for reliable prediction. Equation 1 is a mathematical relationship that expresses the effect of temperature and AFBN inputs on G*/sinδ. The coded equation is useful for identifying the relative impact of the factors by comparing the factor coefficients. RSM plots are given in Fig. 12.

$$\begin{aligned} Sqrt(G/\sin\delta) = {} & +59.67 - 37.26^{*}A - 11.08^{*}B \\ & + 0.8823^{*}AB + 11.69^{*}A^2 - 8.28^{*}B^2 \\ & + 3.71^{*}AB^2 + 9.14^{*}B^3 \end{aligned} \quad (1)$$

Table 7 ANOVA results of RSM analysis

Source	Sum of Squares	df	Mean Square	F-value	*p*-value	
Model	14,397.36	7	2056.77	176.58	< 0.0001	Significant
A:Temperature	5789.86	1	5789.86	497.09	< 0.0001	
B:AFBN ratio	194.39	1	194.39	16.69	0.0015	
AB	4.67	1	4.67	0.4011	0.5384	
A^2	539.69	1	539.69	46.33	< 0.0001	
B^2	260.58	1	260.58	22.37	0.0005	
AB^2	43.28	1	43.28	3.72	0.0779	
B^3	176.63	1	176.63	15.16	0.0021	
Residual	139.77	12	11.65			
Cor Total	14,537.13	19				
Std. Dev	3.41		R^2	0.9904		
Mean	62.58		Adjusted R^2	0.9848		
C.V. %	5.45		Predicted R^2	0.965		
			Adeq Precision	37.9513		

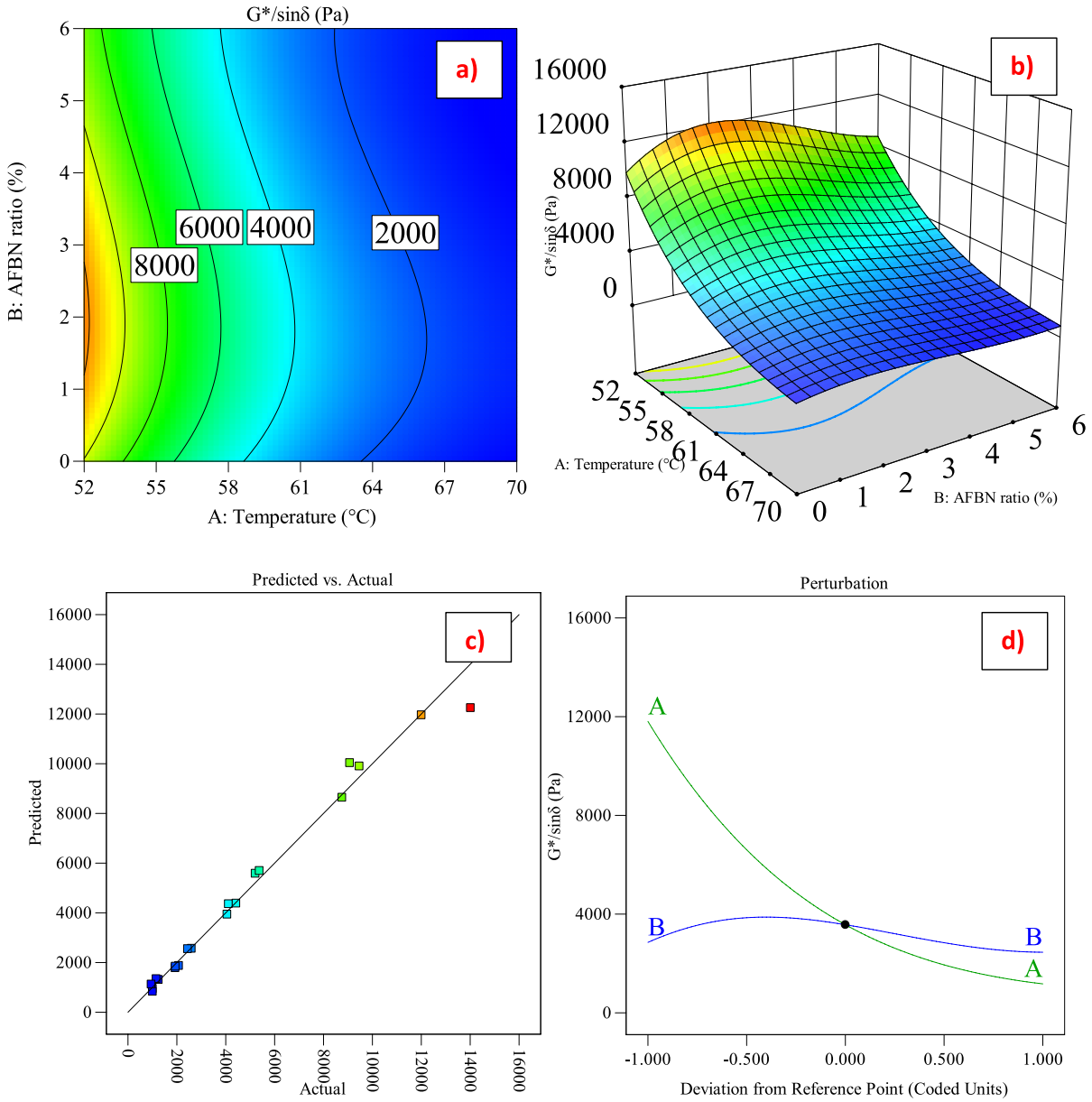


Fig. 12 RSM plots for G*/sinδ values

In Fig. 12, the response surface analysis for the rheological parameter G*/sinδ, the contour distribution, the comparison of the predicted and observed values and the perturbation diagram showing the effect of the factors are presented. In Fig. 12a, the effect of the interaction between temperature (A) and AFBN ratio (B) on G*/sinδ (Pa) is shown via the two-dimensional contour diagram. The G*/sinδ value represents the elastic character of the asphalt binder and its resistance to deformation, and high values indicate high-performance binders. When the graph is examined, it is observed that the G*/sinδ value decreases significantly with the increase in temperature. This reveals the dominant effect of temperature on the viscoelastic behavior of the binder. While the increase in the AFBN ratio initially has a positive effect on G*/sinδ, it is seen that this positive effect

decreases and sometimes reverses as the additive ratio increases above 2%. This shows that when the AFBN additive is used at the optimum rate (2%), it increases the elastic modulus of the binder; but it shows that it can weaken the rheological structure at higher rates.

Figure 12b illustrates the combined effect of temperature and AFBN ratio on G*/sinδ through a three-dimensional response surface. The results show that increasing temperature significantly reduces binder stiffness, while increasing the AFBN content up to 2% enhances G*/sinδ. However, beyond 2% AFBN, a decline in G*/sinδ is observed, indicating that excessive additive content adversely affects binder performance. Figure 12c compares the model-predicted and experimental G*/sinδ values, showing a close alignment along the regression line, which confirms the high predictive accuracy of the model and is consistent with the high R^2 value (0.9904) obtained from ANOVA. The perturbation plot in Fig. 12d reveals that temperature has a much stronger and more dominant negative effect on G*/sinδ than the AFBN ratio. While the additive provides a positive contribution, this effect is limited to a narrow range (0–2%) and diminishes beyond the optimum level. Overall, the model is both statistically sound and rheologically meaningful, demonstrating that an AFBN content of approximately 2% provides the optimum improvement in high-temperature elastic performance, whereas higher ratios may impair structural integrity.

Within the scope of the RSM analysis, numerical optimization was performed to evaluate the combined effects of temperature and AFBN ratio on rutting resistance. Numerical optimization aims to identify the factor combinations that best satisfy predefined objectives; in this study, temperature and AFBN ratio limits were defined to maximize the G*/sinδ value. Design-Expert software applied desirability functions to determine the optimal factor levels. The optimization focused on the most critical condition of 70 °C, where rutting risk is highest, and the AFBN ratio was examined within the range of 1–3%, based on experimental observations indicating optimal performance around 2% AFBN.

Table 8 shows different optimization scenarios for AFBN ratio at 70 °C. When Table 8 is examined, the three highest G*/sinδ values among the scenarios were determined in scenarios 2, 4 and 15. Among these, the scenario with the lowest additive content was determined as scenario 15, with no obvious difference in rutting performance. According to Table 8,

Table 8 Optimization solutions for ideal AFBN ratio

Number	Temperature	AFBN ratio	G*/sinδ	Desirability	
1	70	2.308	1314.805	1	
2	*70*	*1.691*	*1374.926*	*1*	
3	70	1.863	1366.887	1	
4	*70*	*1.599*	*1376.019*	*1*	
5	70	1.335	1365.347	1	
6	70	1.77	1372.16	1	
7	70	1.154	1345.237	1	
8	70	2.574	1266.947	1	
9	70	2.192	1332.187	1	
10	70	1.416	1370.904	1	
11	70	2.793	1221.386	1	
12	70	2.094	1344.827	1	
13	70	2.508	1279.688	1	
14	70	2.4	1299.482	1	
15	70	1.49	1374.185	1	Selected
16	70	1.946	1360.333	1	
17	70	2.924	1191.924	1	
18	70	2.992	1176.46	1	
19	70	2.689	1243.661	1	
20	70	2.021	1353.105	1	

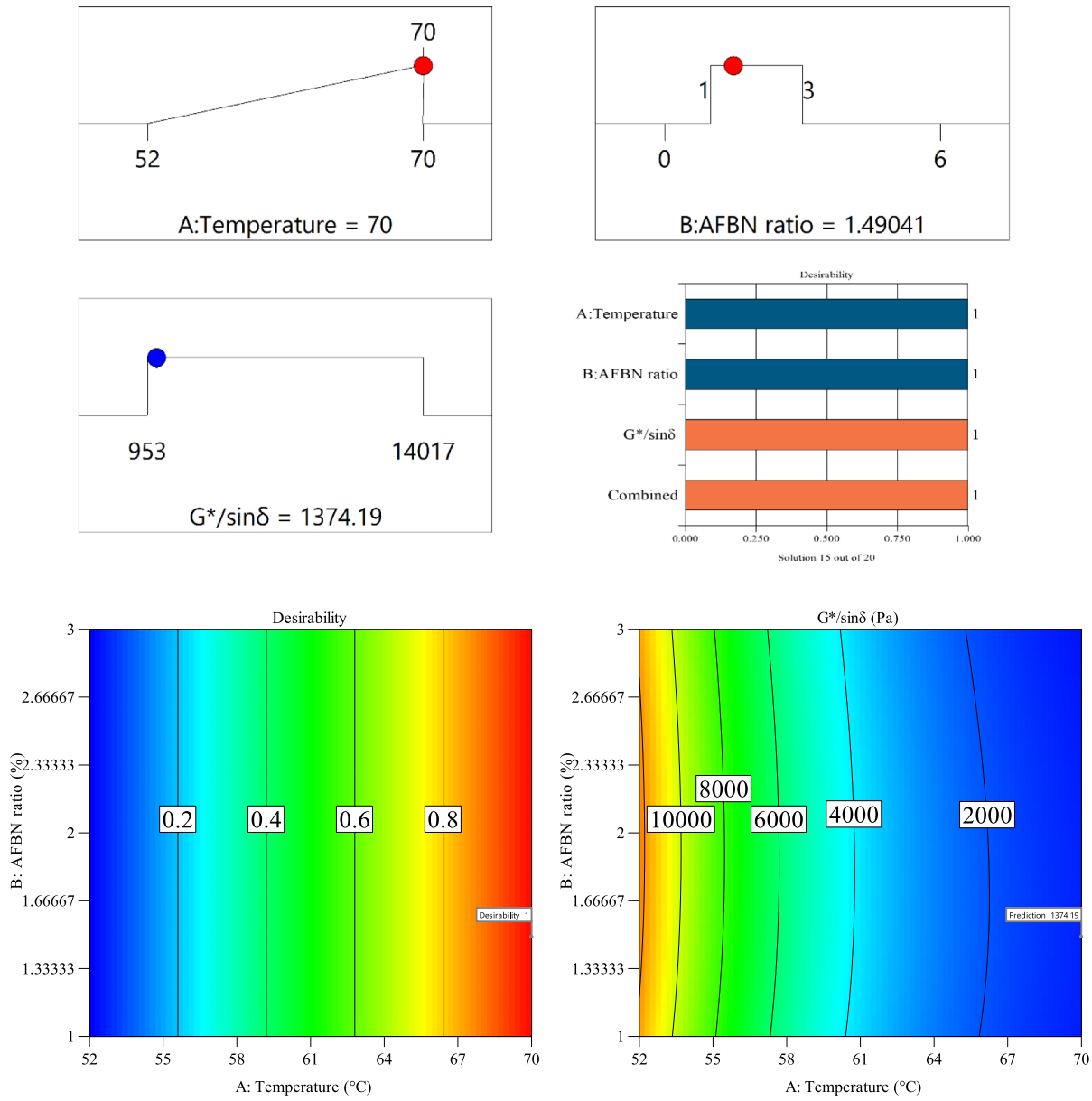


Fig. 13 RSM optimization plots

it can be said that the ideal AFBN ratio is approximately 1.5%. Optimization plots are given in Fig. 13.

Figure 13 illustrates the RSM optimization results obtained at a constant temperature of 70 °C, allowing the isolated evaluation of the AFBN additive ratio on binder rheological performance. The optimization identified an optimum AFBN ratio of 1.49%, at which the G*/sinδ value reached 1374.19 Pa, indicating maximized resistance to permanent deformation under high-temperature conditions. This result demonstrates that the additive is most effective at an optimum level and that higher ratios do not further improve performance. The findings challenge the assumption that maximum performance occurs at a 2% additive content and show that a lower ratio can provide superior performance when supported by statistical modeling. Moreover, the desirability analysis yielded a combined desirability value of 1.0, confirming that the selected optimization point satisfies all objective

functions simultaneously and highlighting the reliability of the model. Overall, the results confirm that RSM-based optimization enables both performance enhancement and material efficiency in asphalt binder design. Figure 16 presents contour graphs for the optimization study.

In Fig. 13, two-dimensional contour diagrams showing the effects of AFBN additive ratio on the rheological performance (G*/sinδ) and optimization suitability score (desirability) of the binder under conditions where the temperature parameter is kept constant at 70 °C are presented.

Figure 13 bottom-left shows the contour distribution of the desirability function (suitability value). This graph reflects the degree to which the system provides satisfactory results as a result of multi-objective optimization carried out in line with certain targets. As can be seen, while the suitability score is at the minimum level at 1% additive ratio, a desirability value of approximately 0.8 is reached when the additive ratio reaches 1.49%. This finding shows that when AFBN additive is used at 1.49%, the highest level of compliance is achieved with both the rheological performance criteria of the binder and the economic efficiency targets. The fact that the desirability value converges to 1 reveals that the optimization result is ideal in both technical and practical terms.

Figure 13 (bottom-right) illustrates the combined effect of temperature and AFBN additive ratio on the G*/sinδ parameter, which reflects the elastic stiffness and rutting resistance of the asphalt binder at high temperatures. The results show a pronounced decrease in G*/sinδ with increasing temperature, indicating progressive weakening of the binder's viscoelastic structure. At a constant temperature of 70 °C, the G*/sinδ value reaches a maximum of 1374.19 Pa at an AFBN content of 1.49%, in agreement with the optimization results. However, further increasing the additive ratio to 2.5–3% leads to a reduction in G*/sinδ, suggesting that excessive additive content adversely affects rheological performance. Overall, the contour plots demonstrate that precise optimization of the additive ratio is critical, with 1.49% AFBN providing the optimum balance between additive efficiency, high desirability, and enhanced deformation resistance.

4 Conclusions

In this study, a novel asphalt binder additive (AFBN) was synthesized from waste tallow, 1,6-diaminohexane, and hexagonal boron nitride (h-BN) to enhance high-temperature performance and aging resistance. The additive was produced using low-cost and sustainable raw materials, and its chemically reactive structure was confirmed by FT-IR, ^{1}H-NMR, and ^{13}C-NMR analyses. FT-IR spectra showed the disappearance of ester C=O bands and the formation of amide C=O and N–H stretching bands, while ^{1}H-NMR D_2O exchange and TFA protonation experiments verified the presence of free amide protons. These results clearly confirm successful amidation and indicate the potential for electrostatic B-N–N interactions with h-BN.

Thermogravimetric analysis (TGA) demonstrated that the AFBN additive possessed adequate thermal stability, showing no decomposition at the asphalt modification temperature of 160 °C. The inclusion of h-BN was found to delay the onset of thermal degradation and improve the residual mass at high temperatures, further reinforcing the additive's suitability for high-temperature mixing and storage.

The produced additive was incorporated into asphalt binders at varying ratios (1%, 2%, 4%, and 6%) and evaluated through both conventional binder tests and advanced rheological characterization. Results from penetration and softening point tests revealed that the use of AFBN improved binder stiffness and thermal resistance, with 2% AFBN offering the most favorable balance. Rotational viscosity measurements further confirmed that this additive increased viscosity at both 135 °C and 165 °C while remaining within Superpave limits, indicating better workability control and thermal deformation resistance.

Dynamic Shear Rheometer (DSR) tests conducted before and after RTFOT aging showed that AFBN-modified binders, especially those with 2% additive, had significantly improved G/sinδ* values and reduced phase angles (δ), pointing to enhanced rutting resistance and elastic behavior. Post-RTFOT analysis confirmed that the additive improved aging resistance by limiting hardening (as shown by softer penetration drops and higher softening points compared to unmodified binders). The *2% AFBN binder retained the highest post-aging G/sinδ value (4300 Pa at 70 °C)**, outperforming all other samples.

A significant outcome of this work is the integration of Response Surface Methodology (RSM) and desirability-based numerical optimization, which identified 1.49% AFBN as the optimal dosage at

70 °C, maximizing G*/sinδ to 1374.19 Pa with a desirability index of 1.0. Although 2% AFBN appeared optimal in experimental trials, optimization models revealed that a lower additive dosage can yield equivalent or better rheological performance, contributing to both cost-efficiency and sustainability.

In summary, this study shows that a waste-derived, chemically engineered amido-boron additive can be successfully synthesized and used to improve the high-temperature performance and aging resistance of asphalt binders. The combined use of chemical characterization (FT-IR, ^{1}H-NMR, ^{13}C-NMR), thermal analysis (TGA), rheological evaluation (DSR, RV), and numerical optimization (RSM) provides a robust framework for the development of next-generation asphalt modifiers. The results demonstrate both performance enhancement and resource efficiency, and offer a strong basis for future studies focusing on field performance, moisture damage, and low-temperature cracking behavior of AFBN-modified asphalt systems. Future work will include extended frequency-temperature sweep testing to construct master curves and to evaluate cracking-related rheological indices such as ΔTc and the Glover-Rowe parameter, enabling a more comprehensive low- and intermediate-temperature performance assessment.

Acknowledgements This study was supported and funded by Bursa Technical University Scientific Research Project (BTU-BAP, Project No:231N006).

Funding Open access funding provided by the Scientific and Technological Research Council of Türkiye (TÜBİTAK). Bursa Technical University Scientific Research Project, BTU-BAP 231N006, Bahadır Yılmaz.

Data availability Data will be available on reasonable request.

Declarations

Conflict of interset The authors have no relevant financial or non-financial interests to disclose.

Open Access This article is licensed under a Creative Commons Attribution 4.0 International License, which permits use, sharing, adaptation, distribution and reproduction in any medium or format, as long as you give appropriate credit to the original author(s) and the source, provide a link to the Creative Commons licence, and indicate if changes were made. The images or other third party material in this article are included in the article's Creative Commons licence, unless indicated otherwise in a credit line to the material. If material is not included in the article's Creative Commons licence and your intended use is not permitted by statutory regulation or exceeds the permitted use, you will need to obtain permission directly from the copyright holder. To view a copy of this licence, visit http://creativecommons.org/licenses/by/4.0/.

References

1. Ministry of Environment and Urbanisation (2019) Regulation on the Management of Waste Oils. Official Gazette of the Republic of Turkey 30985
2. Ndiaye M, Arhaliass A, Legrand J et al (2020) Reuse of waste animal fat in biodiesel: biorefining heavily-degraded contaminant-rich waste animal fat and formulation as diesel fuel additive. Renew Energy 145:1073–1079. https://doi.org/10.1016/j.renene.2019.06.030
3. Mustafa Ertunc Tat, Jon H. Van Gerpen, Paul S. Wang (2004) Fuel property effects on injection timing, ignition timing and oxides of nitrogen emissions from biodiesel-fueled engines. In: 2004, Ottawa, Canada August 1 - 4, 2004. American Society of Agricultural and Biological Engineers, St. Joseph, MI
4. McCormick RL, Graboski MS, Alleman TL et al (2001) Impact of biodiesel source material and chemical structure on emissions of criteria pollutants from a heavy-duty engine. Environ Sci Technol 35:1742–1747. https://doi.org/10.1021/es001636t
5. Furia TE (1973) CRC handbook of food additives, Second Edition. Taylor \& Francis
6. Andreo-Martínez P, Ortiz-Martínez VM, Salar-García MJ et al (2022) Waste animal fats as feedstock for biodiesel production using non-catalytic supercritical alcohol transesterification: a perspective by the PRISMA methodology. Energy Sustain Dev 69:150–163. https://doi.org/10.1016/j.esd.2022.06.004
7. Pešek K (2011) Atherosclerotic cardiovascular disease. IntechOpen, Rijeka
8. Malins C (2023) The impact of biofuel demand on the European market for rendered animal fats. Cerulogy 1–38
9. Feddern V, Cunha A, De Pra MC, et al (2011) Animal fat wastes for biodiesel production. In: Biodiesel - feedstocks and processing technologies. InTech
10. Aslan FB, Murtezaoğlu K, Melikoğlu M (2024) Techno-economic analysis and calculation of environmental impacts of biodiesel production from animal fat wastes in Turkey. J Fac Eng Archit Gazi Univ 39:2077–2090. https://doi.org/10.17341/gazimmfd.1265052
11. Valente AL, Massulo Aguiar MF, Baia ACF et al (2025) Process analysis of waste animal fat pyrolysis and fractional distillation in semi-batch reactors: influence of temperature and reaction time. Energies 18:4517. https://doi.org/10.3390/en18174517
12. Xu P, Hu Q, Tang J et al (2024) Laboratory evaluation of the rejuvenation efficiency of biomass-derived phenolic oil on the asphalt binder with various aging conditions. Mater Struct 57:156. https://doi.org/10.1617/s11527-024-02434-7
13. Sun Z, Yi J, Chen Z et al (2019) Chemical and rheological properties of polymer modified bitumen incorporating bio-oil derived from waste cooking oil. Mater Struct 52:106. https://doi.org/10.1617/s11527-019-1400-7

14. Xintao Z, Meizhu C, Yuechao Z et al (2022) Influence of macromolecular substances in waste cooking oil on rejuvenation properties of asphalt with different aging degrees. Constr Build Mater 361:129522. https://doi.org/10.1016/j.conbuildmat.2022.129522
15. Xu N, Wang H, Wang H et al (2023) Research progress on resource utilization of waste cooking oil in asphalt materials: a state-of-the-art review. J Clean Prod 385:135427. https://doi.org/10.1016/j.jclepro.2022.135427
16. Chen A, Hu Z, Li M et al (2021) Investigation on the mechanism and performance of asphalt and its mixture regenerated by waste engine oil. Constr Build Mater 313:125411. https://doi.org/10.1016/j.conbuildmat.2021.125411
17. Aliyu Yaro NS, Sutanto MH, Habib NZ et al (2022) Application and circular economy prospects of palm oil waste for eco-friendly asphalt pavement industry: a review. J Road Eng 2:309–331. https://doi.org/10.1016/j.jreng.2022.10.001
18. Tosun HB (2023) Production and characterisation of waste tire pyrolytic oil – Investigating physical and rheological behaviour of pyrolytic oil modified asphalt binder. Heliyon 9:e12851. https://doi.org/10.1016/j.heliyon.2023.e12851
19. Feng L, Liu J, Hu L (2023) Rheological behavior of asphalt binder and performances of asphalt mixtures modified by waste soybean oil and lignin. Constr Build Mater 362:129735. https://doi.org/10.1016/j.conbuildmat.2022.129735
20. Yan K, Peng Y, You L (2020) Use of tung oil as a rejuvenating agent in aged asphalt: laboratory evaluations. Constr Build Mater 239:117783. https://doi.org/10.1016/j.conbuildmat.2019.117783
21. Nogueira RL, Soares JB, Soares SdeA (2019) Rheological evaluation of cotton seed oil fatty amides as a rejuvenating agent for RAP oxidized asphalts. Constr Build Mater 223:1145–1153. https://doi.org/10.1016/j.conbuildmat.2019.06.128
22. Nciri N, Kim N (2024) From bin to binder: Unleashing waste butter's potential as a pioneering bio-modifier for sustainable asphalt engineering. Sustainability 16:4774. https://doi.org/10.3390/su16114774
23. Nciri N, Shin T, Kim N et al (2020) Towards the use of waste pig fat as a novel potential bio-based rejuvenator for recycled asphalt pavement. Materials 13:1002. https://doi.org/10.3390/ma13041002
24. Anyaogu ID, Ejikeme PM, Ibemesi JA (2010) Development of thixotropic coatings using dimerized soybean oil fatty acids: the case of polyamide of 1,2-phenylene diamine. J Polym Environ 18:104–115. https://doi.org/10.1007/s10924-010-0160-9
25. Alam M, Ray AR, Ashraf SM, Ahmad S (2009) Synthesis, characterization and performance of amine modified linseed oil fatty amide coatings. J Am Oil Chem Soc 86:573–580. https://doi.org/10.1007/s11746-009-1375-6
26. de Andrade Souza L, Moreira DR, Ricardo NMPS et al (2023) Esters from castor oil functionalized with aromatic amines as a potential lubricant. J Am Oil Chem Soc 100:175–184. https://doi.org/10.1002/aocs.12648
27. Boykin R. O., Glendale, S., Osborne PS (1964) Neutron absorbing asphaltic composition
28. Marzocchi A., Roberts, G. M., Bolen CE (1982) Boron modified asphalts
29. Oruç Ş, Yılmaz B, Sancak K (2022) Characterization and rheological behavior of asphalt binder modified by a novel cyclic borate ester additive. Constr Build Mater 348:128673. https://doi.org/10.1016/j.conbuildmat.2022.128673
30. Oruç Ş, Yılmaz B, Sancak K (2016) Effect of boron-containing additives on rheological properties of asphalt binder. Road Mater Pavement Des 17:810–824. https://doi.org/10.1080/14680629.2015.1120228
31. Liu Z, Dibaji A, Li D et al (2021) Challenges and solutions in surface engineering and assembly of boron nitride nanosheets. Mater Today 44:194–210. https://doi.org/10.1016/j.mattod.2020.11.020
32. Lu T, Wang L, Jiang Y et al (2016) Hexagonal boron nitride nanoplates as emerging biological nanovectors and their potential applications in biomedicine. J Mater Chem B 4:6103–6110. https://doi.org/10.1039/C6TB01481J
33. Zhang H, Liu Y, Sun K et al (2023) Applications and theory investigation of two-dimensional boron nitride nanomaterials in energy catalysis and storage. EnergyChem 5:100108. https://doi.org/10.1016/j.enchem.2023.100108
34. Li Z, Wu S (2025) Research on the heat conduction, physical and rheological properties of asphalt binder modified with boron nitride. Constr Build Mater 462:139937. https://doi.org/10.1016/j.conbuildmat.2025.139937
35. Yero SA, Hainin MR (2012) Viscosity characteristics of modified bitumen. ARPN J Sci Technol 2:500–503
36. Yilmaz B, Ozdemir AM, Gürbüz HE (2022) Assessment of thermal properties of nanoclay-modified bitumen. Arab J Sci Eng. https://doi.org/10.1007/s13369-022-07142-4
37. Ulucan M, Alyamac KE (2022) A holistic assessment of the use of emerging recycled concrete aggregates after a destructive earthquake: mechanical, economic and environmental. Waste Manag 146:53–65. https://doi.org/10.1016/j.wasman.2022.04.045
38. Özdemir AM (2025) Experimental evaluation and 3D finite element simulation of creep behaviour of SBS modified asphalt mixture. Constr Build Mater 460:139821. https://doi.org/10.1016/j.conbuildmat.2024.139821
39. Ulucan M (2024) From waste to sustainable production: experimental design and optimization of sustainable concrete using response surface methodology and life cycle assessment. Sustain Chem Pharm 42:101770. https://doi.org/10.1016/j.scp.2024.101770
40. Cheng X, Blake GM, Brown JK et al (2017) The measurement of liver fat from single-energy quantitative computed tomography scans. Quant Imaging Med Surg. https://doi.org/10.21037/qims.2017.05.06
41. Solozhenko VL, Le Godec Y, Klotz S et al (2002) In situ studies of boron nitride crystallization from BN solutions in supercritical N-H fluid at high pressures and temperatures. Phys Chem Chem Phys 4:5386–5393. https://doi.org/10.1039/b206005a
42. Ysiwata-Rivera AP, Hernández-Hernández E, Cadenas-Pliego G et al (2020) Effect of modified hexagonal boron nitride nanoparticles on the emulsion stability, viscosity and electrochemical behavior of nanostructured acrylic coatings for the corrosion protection of AISI 304 stainless

steel. Coatings 10:488. https://doi.org/10.3390/coatings10050488
43. Kostoglou N, Polychronopoulou K, Rebholz C (2015) Thermal and chemical stability of hexagonal boron nitride (h-BN) nanoplatelets. Vacuum 112:42–45. https://doi.org/10.1016/j.vacuum.2014.11.009

Publisher's Note Springer Nature remains neutral with regard to jurisdictional claims in published maps and institutional affiliations.